This is a preprint, the final version is subject to change, of the American Mineralogist (MSA)
Cite as Authors (Year) Title. American Mineralogist, in press.
(DOI will not work until issue is live.) DOI: http://dx.doi.org/10.2138/am-2017-5909

REVISION 1

Thermodynamics and crystal chemistry of rhomboclase, $(H_5O_2)Fe(SO_4)_2 \cdot 2H_2O$, and the phase $(H_3O)Fe(SO_4)_2$

JURAJ MAJZLAN[1,*], KLAUS-DIETER GREVEL[1], BORIS KIEFER[2], ULLA GRO NIELSEN[3], ELISABETH GRUBE[3,4], EDGAR DACHS[5], ARTUR BENISEK[5], MARY ANNE WHITE[6], MICHEL B JOHNSON[6]

[1]Institute of Geosciences, Friedrich-Schiller-University, Carl-Zeiss Promenade 10, D-07745 Jena, Germany
[2]Department of Physics, 153 Gardiner Hall, New Mexico State University, Las Cruces 88003, New Mexico, USA
[3]Department of Physics, Chemistry, and Pharmacy, University of Southern Denmark, Campusvej 55, 5230 Odense M, Denmark
[4]Current address: Interdisciplinary Nanoscience Center and Department of Chemistry, Aarhus University, Langelandsgade 140, 8000 Århus C, Denmark
[5]Department of Chemistry and Physics of Materials, Division Mineralogy, University of Salzburg, Hellbrunnerstrasse 34, A-5020 Salzburg, Austria
[6]Department of Chemistry and Institute for Research in Materials, Dalhousie University, Halifax, NS B3H 4R2, Canada

*Corresponding author:
Institute of Geosciences
Friedrich-Schiller-University
Carl-Zeiss Promenade 10
D-07745 Jena, Germany
Telephone: +49-3641-948700
Fax: +49-3641-948602
e-mail: Juraj.Majzlan@uni-jena.de

Submitted: *American Mineralogist*, July 5, 2016
Reviews received: September 6, 2016
Revision 1 submitted: September 22, 2016

Always consult and cite the final, published document. See http:/www.minsocam.org or GeoscienceWorld

ABSTRACT – The system Fe_2O_3-SO_3-H_2O contains the most important minerals of acid mine drainage (AMD), iron oxides and iron sulfates. For geochemical modeling of the AMD systems, reliable thermodynamic data for these phases are needed. In this work, we have determined thermodynamic data for the most acidic sulfates rhomboclase [$(H_5O_2)Fe(SO_4)_2\cdot 2H_2O$ or $(H_3O)Fe(SO_4)_2\cdot 3H_2O$] and the phase $(H_3O)Fe(SO_4)_2$. The actual compositions of the studied phases are $(H_3O)_{1.34}Fe(SO_4)_{2.17}(H_2O)_{3.06}$ (molecular mass of 344.919 $g\cdot mol^{-1}$) and $(H_3O)_{1.34}Fe(SO_4)_{2.17}$ (289.792 $g\cdot mol^{-1}$). Structural details for both phases were refined from synchrotron powder X-ray diffraction data. Enthalpies of formation were determined by acid-solution calorimetry. Low-temperature heat capacity was measured for rhomboclase by relaxation calorimetry but a critical analysis of entropies for a number of oxysalts showed that these data are too high. Entropies for both phases were estimated from a Kopp-rule algorithm. The enthalpies of formation and entropies were combined with previously published temperature-relative humidity brackets to generate an internally consistent thermodynamic data set for rhomboclase: $\Delta_f H^o = -3202.03$ $kJ\cdot mol^{-1}$, $S^o = 378.7$ $J\cdot mol^{-1}\cdot K^{-1}$; and for $(H_3O)_{1.34}Fe(SO_4)_{2.17}$: $\Delta_f H^o = -2276.25$ $kJ\cdot mol^{-1}$, $S^o = 253.2$ $J\cdot mol^{-1}\cdot K^{-1}$. Solubility experiments at room temperature and at $T = 4$ ºC agree well with previously reported data in the system Fe_2O_3-SO_3-H_2O. An inspection of the extended Pitzer model for Fe(III)-SO_4 solutions shows that this model reproduces the general topology of the phase diagram but the position of the calculated solubility curves deviates substantially from the experimental data. Solid state ^2H MAS NMR spectra on deuterated rhomboclase show two isotropic chemical shifts $\delta_{iso}(^2H)$ = of 8±1 and 228±1 ppm, assigned to $D_5O_2^+$ and Fe-OD_2 groups, respectively. Canonical ensemble (NVT) molecular dynamics simulations for $(H_3O)Fe(SO_4)_2$ at T = 300 K showed that the H_3O^+ groups maintain their trigonal pyramidal geometry and perform different types of motion.

KEY WORDS: rhomboclase; acid mine drainage; thermodynamics; hydrogen mobility

Always consult and cite the final, published document. See http:/www.minsocam.org or GeoscienceWorld

INTRODUCTION

The system Fe_2O_3-SO_3-H_2O comprises the most common and important minerals of acid-mine drainage (AMD), a global environmental problem related to mining of ores of metals (e.g., Au, Cu), metalloids (e.g., Sb) and coal, polluting thousands of kilometers of rivers worldwide (Blowes et al. 2003). A number of remediation options have been proposed for various AMD systems, ranging from large volumes with intermediate pollution to relatively small volumes with extreme water compositions (Nordstrom et al. 2000; Johnson and Hallberg 2005; Sheoran and Sheoran 2006; Byrne et al. 2012; Anawar 2015). Early recognition of the vital role of microorganisms in the sustainable formation of AMD (Lacey and Lawson 1970; Nordstrom 1982; Nordstrom and Southam 1997) led to a number of studies on the geomicrobiology of these systems (Hallberg 2010; Klein et al. 2014; Garris et al. 2016). Significant attention is paid to the possibility of predicting the development of AMD (Parbhakar-Fox and Lottermoser 2015) so that measures can be taken before the problem unfolds in a way that is difficult and costly to manage and remediate.

An integral part of the research and remediation of AMD systems is geochemical modeling (Perkins et al. 1995), using the known thermodynamic and kinetic parameters for the phases involved in the AMD systems. Forward simulations can predict the time evolution of an AMD system or the performance of a remediation measure. Inverse simulation can explain the path of the aqueous fluids between uncontaminated surface or underground water or precipitation and acidic, metal-loaded fluids. For such simulations, the information about the solids forming or dissolving is crucial. Mineralogy of the AMD systems is well known from both laboratory (Bigham et al. 1996; Sejkora et al. 2015) and field studies (Nordstrom et al. 2000; Buckby et al. 2003). The AMD minerals include iron oxides (a generic term for the group of oxides, hydroxides, and oxyhydroxides of ferric iron) and ferric sulfates. Thermodynamic data for the iron oxides are known fairly well and were subject to several critical reviews (Lemire et al. 2013 and references therein). Ferric sulfates, on the other hand, lag somewhat behind. While some of the relevant data are available (Stoffregen 1993; Baron and Palmer 1996; Jerz and Rimstidt 2003; Majzlan et al. 2006, and others), gaps and inconsistencies within the available dataset introduce large uncertainties in the geochemical models of AMD systems.

Always consult and cite the final, published document. See http:/www.minsocam.org or GeoscienceWorld

Solubility and phase relationships among the ferric sulfates were a subject of many early studies (Recoura 1907; Cameron and Robinson 1907; Wirth and Bakke 1914; Posnjak and Merwin 1922; Appleby and Wilkes 1922; Baskerville and Cameron 1935; Koerker and Calderwood 1938). Ferric sulfates were divided into basic, normal, and acidic, depending on the Fe/S ratio and the nature of the H-bearing moieties in the structures. Hydronium jarosite, $(H_3O)Fe^{3+}_3(SO_4)_2(OH)_6$), and ferricopiapite, $Fe^{3+}_{14/3}(SO_4)_6(OH)_2{\cdot}20(H_2O)$, are the basic ferric sulfates. The normal sulfates include the entire series of the $Fe_2(SO_4)_3{\cdot}nH_2O$ phases. Rhomboclase, $(H_5O_2)Fe(SO_4)_2{\cdot}2H_2O$, is the acidic ferric sulfate. All these minerals precipitate from acidic to very acidic aqueous solutions and the terms basic, normal, and acidic refer to their composition in solid state.

The structural formula of rhomboclase $(H_5O_2)Fe(SO_4)_2{\cdot}2H_2O$ reflects the existence of the $(H_5O_2)^+$ ions in its interlayer. In this work, however, we will prefer to use the formula $(H_3O)Fe(SO_4)_2{\cdot}3H_2O$ which documents better the relationship of rhomboclase to the acidic phase $(H_3O)Fe(SO_4)_2$.

In this work, we focus on the most acidic portion of the Fe_2O_3-SO_3-H_2O system at ambient temperatures (T < 30 °C), represented by rhomboclase and the phase $(H_3O)Fe(SO_4)_2$ (not known from nature). This study complements the classical investigation of this system by Posnjak and Merwin (1922) at temperatures of T = 50 °C and higher. Merwin and Posnjak (1937) attempted to estimate the phase relationships at T = 30-40 °C from the observation of natural assemblages. Our work is a synthesis of thermodynamic data (enthalpies of formation and estimated standard entropies) with solubility measurements (performed within this study and literature values), equilibria in temperature-relative air humidity space (Xu et al. 2010), and the Pitzer model for concentrated Fe(III)-SO_4 aqueous solutions (Tosca et al. 2007). The goal of this work was to generate an internally consistent set of thermodynamic data which can be used to model and predict simple AMD systems (i.e., those without additional components) by mathematical analysis optimization of the thermodynamic data at hand. The phase $(H_3O)Fe(SO_4)_2$ is of little interest for the mineralogy of AMD systems as it requires extremely concentrated sulfuric acid solutions to precipitate. The data for this phase were needed to refine the thermodynamic properties of rhomboclase and therefore also determined.

Always consult and cite the final, published document. See http:/www.minsocam.org or GeoscienceWorld

In addition, we have investigated the crystal chemistry of rhomboclase and the acidic phase $(H_3O)Fe(SO_4)_2$ in the studied system, especially with respect to the nature and mobility of the H atoms. Their mobility is of interest in materials science because rhomboclase and related phases were studied in the past as potential proton conductors (Brach and Goodenough 1988). Rhomboclase was studied by solid-state deuterium (^2H) nuclear magnetic resonance (NMR) spectroscopy. Further complexity of this phase and its ability to take up arsenic in its structure were recently reported by Bolanz et al. (2016). Because of severe experimental difficulties, the phase $(H_3O)Fe(SO_4)_2$ could be investigated only by *ab-initio* molecular dynamics simulations. This phase has a tendency to absorb H_2O, release H_2SO_4, and aggressively etch all materials with which it comes into contact. It is difficult to store, transport, and maintain this compound in a phase-pure state. Therefore, our experiments on this phase were restricted to acid-solution calorimetry where phase purity was maintained at least for the short duration of our measurements.

METHODS AND MATERIALS

A series of charges was prepared by mixing 96 % H_2SO_4, fine-grained, homogeneous hydrated ferric sulfate $[Fe_2(SO_4)_3 \cdot xH_2O]$, (reagent grade, Alfa Aesar), and water. The two former chemicals will be referred to as sulfuric acid and ferric sulfate. The amount of water, x, in the ferric sulfate reagent, was determined to be ~6.75 by a thermogravimetric analysis. The initial compositions of the charges are listed in Tables S1 and S2.

One set of the charges was allowed to stand for 3 years at room temperature (22±3 °C), although they precipitated most of the solids within a few months from preparation. Another set of charges was prepared as follows. The charges were initially allowed to stand for 6 months at room temperature. Afterwards, the liquids were decanted, transferred to new vials and these vials were kept in a refrigerator at 4 °C for five years.

At the end of the experimental period (3-5 years), all charges contained a layer of solid material and liquid. The solid portions were first visually described and the minerals identified by their color, based on our previous experience with this system. This simple identification was verified by polarized-light microscopy where the morphology and the

Always consult and cite the final, published document. See http:/www.minsocam.org or GeoscienceWorld

form of the indicatrix (uniaxial, biaxial) suffices for the identification of the phases. An aliquot of the liquid (2-3 mL) was retrieved with a pipette, filtered through a 0.22 μm hydrophilic polypropylene filter, and diluted with ultrapure 65 % HNO_3 and deionized water. The dilution proceeded on a weight basis such that the molality of the solutions can be calculated after the chemical analyses were returned from the laboratory. The solutions were analyzed for Fe and S by inductively-coupled plasma optical emission spectrometry (ICP-OES) with a Varian 725 ICP-OES with a charge-couple device (CCD) detector (University of Jena). Afterwards, a small portion of the solid was removed with a pipette, applied immediately onto a zero-background silicon holder, and subjected to a powder X-ray diffraction analysis (XRD). These experiments confirmed without exception the visual and polarized-light identification of the minerals.

The deuterated sample for NMR spectroscopy was prepared by mixing of 3.62 g D_2O, 1.42 mL H_2SO_4, and 0.761 g $Fe_2(SO_4)_3 \cdot xH_2O$. The sample was allowed to stand at room temperature in a sealed bottle for 6 months. Afterwards, the solid was separated from the liquid by filtration, quickly washed with a small amount of D_2O, allowed to dry in air and transported sealed for further measurements.

For the calorimetric work on rhomboclase, the suspension from the sample TB-30 was filtered with a ceramic filter, washed three times with a small amount of pure ethanol, and allowed to dry at room temperature. $(H_3O)Fe(SO_4)_2$ for the XRD and calorimetric work was synthesized by dehydration of rhomboclase in a platinum crucible in an oven at 140 ºC. Both rhomboclase and $(H_3O)Fe(SO_4)_2$ are difficult to handle. They release sulfuric acid and stain all metallic objects which they contact. Particularly $(H_3O)Fe(SO_4)_2$ is not easy to make and prepare for experiments. The $(H_3O)Fe(SO_4)_2$ samples had always consistency of a moist slush owing to the film of sulfuric acid released from the solid. After seven years of trials and errors, we were able to convince ourselves that we possess a good sample for calorimetry even though the sample was never a dry powder.

In-house powder XRD patterns were collected with a Bruker D8 ADVANCE X-ray powder diffractometer, employing Cu Kα radiation, Ni filter, and a Lynxeye 1D detector. The data were collected at room temperature, over angular range of 5° to 60° 2Θ, with step of 0.02° 2Θ, and counting time of 2 seconds per point.

Always consult and cite the final, published document. See http:/www.minsocam.org or GeoscienceWorld

The synchrotron XRD patterns were collected at the bending magnet beamline PDIFF at the synchrotron light source Angströmquelle Karlsruhe (ANKA, Karlsruhe, Germany). X-rays with a wavelength of 0.70423(1) Å were selected by a double crystal Si(111) monochromator. The wavelength and the zero angle of the diffractometer were determined with a NIST SRM 640 silicon (ANKA). The $(H_3O)Fe(SO_4)_2$ slush was loaded into a 1.0 mm capillary and spun at 10,000 rpm for 10 minutes in a centrifuge to force the sample inside the capillary. Rhomboclase samples were loaded into the capillaries with a small funnel. The intensity of the incoming beam was monitored during the data collection by an ion chamber and the measured intensities of the diffracted beam were corrected for the decay and fluctuations of the primary beam. The diffracted beam was analyzed by a Ge(111) crystal and Na(Tl)I scintillation detector. The XRD pattern of $(H_3O)Fe(SO_4)_2$ was collected at room temperature, over angular range of 2.0 to 38.0º 2Θ, with step of 0.002º, and counting time of 2 s per point. The XRD patterns of rhomboclase were collected at room temperature, over angular range of 4.0 to 40.0º 2Θ, with step of 0.005º, and counting time of 1 s per point. The diffraction data were treated with a full-profile Rietveld refinement with the GSAS (General Structure Analysis System) program of Larson and von Dreele (1994).

For the solution calorimetric experiments at T = 25 ºC, we used a commercial IMC-4400 isothermal microcalorimeter (Calorimetry Sciences Corporation) which we modified for the purposes of acid-solution calorimetry. The liquid bath of the calorimeter was held at a constant temperature of 298.15 K with fluctuations smaller than 0.0005 K. The calorimetric solvent was 25 g of deionized water or 25 g of 5 *N* HCl contained in a polyetheretherketone (PEEK) cup with a total volume of 60 mL. The cup was closed with a PEEK screw cap and inserted into the calorimeter well. The calorimeter stabilized after ~8 hours. During the stabilization and the experiment, the solvent was stirred by a SiO_2 glass stirrer by a motor positioned about 40 cm from the active zone of the instrument. The samples were pressed into a pellet and weighed on a micro-balance with a precision of 0.002 mg (as stated by the manufacturer). The pellets were then dropped through a SiO_2 glass tube into the solvent and the heat produced or consumed during the dissolution was measured. The heat flow between the reaction cup and the constant temperature reservoir was then integrated to calculate the caloric effect. A typical experiment lasted

Always consult and cite the final, published document. See http:/www.minsocam.org or GeoscienceWorld

50-60 minutes and the end of the experiment was judged from the return of the baseline to the pre-experiment position. The calorimeter was calibrated by dissolving ~20 mg pellets of KCl in 25 g of deionised water. Prior to each calibration measurement, KCl was heated overnight in the furnace at 800 K to remove the adsorbed water. The expected heat effect for the calibration runs was calculated from Parker (1965).

Heat capacity was measured by relaxation calorimetry using a commercial Physical Properties Measurement System (PPMS, from Quantum Design, San Diego). With due care, accuracy can be within 1% for 5 K to 300 K, and 5% for 0.7 K to 5 K (Kennedy et al. 2007). Due to the hydrated nature of the mineral sample, it needed to be isolated from the vacuum required for heat capacity measurements. Measurements were conducted in the temperature interval 2 to 300 K.

Crystal chemistry of $(H_3O)Fe(SO_4)_2$ was studied by static and molecular dynamic *ab-initio* calculations that are based on density-functional theory (DFT, Hohenberg and Kohn 1964). These calculations make no assumptions on the nature of bonding and provide insights into the crystal chemistry that is independent of the experiment. Thus, our calculations provide an ideal complement to our experimental efforts to determine the hydrogen positions in $(H_3O)Fe(SO_4)_2$. All calculations were performed using the VASP software package (Kresse and Hafner 1993; Kresse and Furthmüller 1996a,b). Electronic correlations were described within the generalized-gradient approximation (GGA) in the parametrization of Perdew, Burke and Ernzerhof (PBE; Perdew et al. 1996). This representation has previously been shown to be more appropriate than the local density approximation (LDA) for hydrogen-bearing systems (Hamann 1997; Tsuchiya et al. 2005; Mookherjee and Stixrude 2006). The interactions between atoms were described within the PAW method (Blöchl 1994; Kresse and Joubert 1999). The results of this approach have been shown to be of comparable accuracy to all electron calculations (Holzwarth et al. 1997; Kresse and Joubert 1999). The core region cut-off radii (1 a_B = 0.529 Å) of the PAW potentials were 2.3 a_B (core configuration $1s^2 2s^2 2p^6 3s^2 3p^6$), 1.9 a_B (core configuration $1s^2 2s^2 2p^6$), 1.52 a_B (core configuration $1s^2$), and 1.1 a_B (no core) for Fe, S, O, and H, respectively.

The canonical ensemble (NVT) molecular dynamic simulations were performed with a planewave cutoff energy of 600 eV, and a single k-point (Γ-point) for a 2x1x1

Always consult and cite the final, published document. See http:/www.minsocam.org or GeoscienceWorld

supercell (60 atoms, 4 H_3O^+ units) that was obtained by doubling the unit cell in the *a*-direction. All dynamic simulations were performed at $T = 300$ K. The temperature was maintained constant throughout the simulations via a Nosé thermostat (Nosé 1984). The thermostat mass was set to 0.075 amu, the equations of motion were integrated using a time step of $\Delta t = 1$ fs, and the shape of the simulation cell was fixed throughout the molecular dynamics simulations.

For the static calculations, we adopted the same plane wave cut-off energy of 600 eV and a *k*-point mesh of 2×1×1 and performed symmetry constraint relaxation to determine the geometric and electronic ground state. Convergence tests showed that these computational parameters are sufficient to obtain solutions of the Kohn-Sham equations (Kohn and Sham 1965) that are converged to within 2.6 meV/atom.

The spin of iron was fixed in its high-spin form (five unpaired electrons) and remained fixed in all calculations. According to Hund's rules, the orbital angular momentum of the ferric iron ($3d^5$) is quenched ($L_z = 0$). Thus, spin-orbit coupling is negligible in high-spin ferric iron compounds and was not included in the present calculations. The absence of a strong coupling was confirmed by the observation of high resolution ^{2}H MAS NMR spectra of rhomboclase, implying fast electron spin relaxation, i.e, paramagnetism.

Solid state ^{2}H MAS NMR spectra were recorded at 11.7 T (77.6 MHz) on a Varian Inova 500 MHz spectrometer using a 3.2 mm HX MAS NMR probe at ambient temperatures. The ^{2}H MAS NMR spectra were referenced to D_2O ($\delta_{iso}(^2H) = 4.6$ ppm). Single pulse spectra were recorded using short pulse angles (< 15°) and 12-20 kHz spinning speed. The ^{2}H MAS NMR spectra were analyzed using STARS.

RESULTS AND DISCUSSION

Solubility measurements

The charges, maintained at room temperature or at $T = 4$ ºC over a long time, precipitated rhomboclase, paracoquimbite, $Fe_2(SO_4)_3 \cdot 9H_2O$; or ferricopiapite, $Fe^{3+}_{14/3}(SO_4)_6(OH)_2 \cdot 20H_2O$. In this work, we will focus on the charges that precipitated rhomboclase; the other ones will be described in more detail in a separate contribution.

Always consult and cite the final, published document. See http:/www.minsocam.org or GeoscienceWorld

Rhomboclase is a prominent acidic ferric sulfate in the system Fe_2O_3-SO_3-H_2O. It is white with yellowish tint, the color being distinct from that of paracoquimbite. In a microscope, rhomboclase is seen as platelets with rhombic outline (Fig. 1). Under crossed nicols, the platelets are not extinct, with intense interference colors, depending on their thickness. Rhomboclase was the only phase found in the charges TB-22 through TB-30. The molalities of the solutions that co-existed with rhomboclase in these charges are listed in Table 1.

Our solubility data for room temperature are in a good agreement with Wirth and Bakke (1914) and Baskerville and Cameron (1935) (Fig. 2). The data also show that the solubility diminishes as temperature decreases. The stability field of rhomboclase is flanked by that of paracoquimbite on the side of lower H_2SO_4 molalities and by the field of $(H_3O)Fe(SO_4)_2$ on the side of higher H_2SO_4 molalities. Coquimbite, predicted to occur at 30-40 ºC in this system by Merwin and Posnjak (1937), was not detected in any of the charges. Paracoquimbite was found in some charges instead.

Crystal structures: powder X-ray diffraction

The powder XRD data confirmed that the samples are pure and suitable for calorimetric investigations. No impurities were detected, either by visual inspection of the regions where they could occur (e.g., the strongest XRD peaks of possible interfering phases) or by the Rietveld refinement.

The principal features of the crystal structure of rhomboclase have been established by Mereiter (1974) and confirmed by Majzlan et al. (2006) and Peterson et al. (2009). No deviations from these models were encountered in this study. The structure of rhomboclase is built by heteropolyhedral layers with $H_5O_2^+$ groups in the interlayer. The occupancies of the some of the O sites in the interlayer, however, appear to be consistently lower than 1 (Mereiter 1974; Majzlan et al. 2006; Peterson et al. 2009). A refinement of the occupancies of the interlayer O atoms from the powder XRD data failed because of strong correlation between several refined parameters. We assumed, that if O occupancy varies, the lattice parameters *c* in the direction perpendicular to the stacking of the layers should also vary. That is, however, not the case (Table 2). Rhomboclase samples synthesized from H_2SO_4 solutions of variable molarity have essentially the same

Always consult and cite the final, published document. See http:/www.minsocam.org or GeoscienceWorld

lattice parameters *c*, implying that the interlayer content does not depend on the properties of the mother liquor.

Crystal structure of $(H_3O)Fe(SO_4)_2$ was solved by Peterson et al. (2009). Starting with their model, we obtained identical polyhedral linkages. Yet, the powder XRD refinement always led a to minimum where the (SO_4) tetrahedra were distorted, with S-O distance varying between 1.35-1.65 Å. Rigid bodies representing the (SO_4) tetrahedra were incorporated in the model several times and the refinement proceeded to a stable minimum with a favorable statistics ($\chi^2 = 9.7$). Once the rigid bodies were removed, however, the refinement produced the same distortion while improving the statistics ($\chi^2 = 5.4$). Restraints on the S-O distances and O-S-O bonding angles mediated this problem only partially.

We note that the trigonal superstructure, that of $(H_3O)Al(SO_4)_2$, contains three octahedral-tetrahedral layers in its unit cell. When viewed in the direction [001], these layers are not superimposed onto each other but offset. To account for this structural feature, we have also created a structural model where the layers in the studied phase $(H_3O)Fe(SO_4)_2$ were offset in an analogous way like those in $(H_3O)Al(SO_4)_2$. The lattice parameters of this model are $a = 4.8064$ Å, $b = 8.3259$ Å, $c = 24.9478$ Å, $\alpha = 70.11°$, $\beta = 90.09°$, $\gamma = 89.96°$. LeBail fits indicated a good agreement between this cell and the experimental pattern. However, attempts to advance with the Rietveld refinement showed similar polyhedral distortion as in the previous model. In addition, this refinement was prone to divergence and suffered from a large number of general atomic positions (72) in the unit cell.

It seems that the powder XRD data, even if they were collected at a synchrotron light source, have too much peak overlap for accurate position determinations for all atoms. It is interesting, however, that only the S-O bonds are affected; the Fe-O bonds and the geometry of the Fe octahedra remain unaltered.

Enthalpies of formation and entropies

Determination of an enthalpy of formation from elements in their standard state ($\Delta_f H^0$) requires the measurement of enthalpies of dissolution of i) samples, and ii) reference phases. Reference phases must be used because a direct measurement of $\Delta_f H^0$ is rarely

Always consult and cite the final, published document. See http:/www.minsocam.org or GeoscienceWorld

possible (for example, for simple oxides by combustion calorimetry). Instead, $\Delta_f H^0$ of the title phases must be derived *via* thermochemical cycles (Table 3) by the application of Hess' law. Hence, the values calculated depend critically on the accuracy of the data for the reference phases, both experimental (calorimetric, this study) and tabulated ($\Delta_f H^0$ of the reference phases).

The reference phases used in this work were MgO, α-$MgSO_4$, γ-FeOOH, and H_2O. The thermodynamic properties of liquid H_2O are believed to be known well. The data for γ-FeOOH were derived with respect to α-Fe_2O_3 (Majzlan et al. 2003) and are considered to be the best data available (Lemire et al. 2013). The data for MgO and α-$MgSO_4$ are also well known. As an additional check for the accuracy of these data, we measured additional enthalpies of dissolution in 5 N HCl (Table 4). The $\Delta_f H^0$ values for all participating phases (CaO, MgO, $CaSO_4$, $MgSO_4$) are known. The calculated enthalpy of the reaction ($\Delta_R H^0_{calc}$) MgO + $CaSO_4$ = CaO + $MgSO_4$ can be compared to the experimentally determined $\Delta_R H^0_{exp}$, based on the dissolution enthalpies of the participating phases. Following this calculation, we obtain $\Delta_R H^0_{exp}$ = 110.4±1.8 kJ·mol^{-1}, $\Delta_R H^0_{calc}$ = 111.2±3.4 kJ·mol^{-1} for the formation enthalpies from the NIST-JANAF tables (Chase 1998) or $\Delta_R H^0_{calc}$ = 112.1±4.3 kJ·mol^{-1} for the formation enthalpies from Robie and Hemingway (1995). The difference of 0.7 kJ·mol^{-1} (NIST-JANAF *versus* our data) is considered to be excellent, the difference of 1.7 kJ·mol^{-1} (Robie and Hemingway 1995 *versus* our data) is satisfactory.

We have used these reference phases in a number of previous studies and obtained excellent results. For example, the enthalpy of formation of monoclinic $Fe_2(SO_4)_3$, measured by this method, is –2585.2±4.9 kJ·mol^{-1} (Majzlan et al. 2005). This value compares fairly well to –2582.0±2.9 kJ·mol^{-1} for the same phase, given in the review of DeKock (1982). We have also shown that α-$MgSO_4$ yields excellent results for the thermodynamics of the $MgSO_4 \cdot nH_2O$ phases (Grevel and Majzlan 2009).

Rhomboclase. The enthalpy of formation of rhomboclase was measured *via* acid-solution calorimetry as –3201.1±2.6 kJ·mol^{-1} for the composition $(H_3O)_{1.34}Fe(SO_4)_{2.17}(H_2O)_{3.06}$ by Majzlan et al. (2006). In that work, the enthalpy of dissolution of rhomboclase in our calorimetric solvent (5 *N* HCl) was 43.7±0.5 J·g^{-1}. A

Always consult and cite the final, published document. See http:/www.minsocam.org or GeoscienceWorld

new sample, synthesized for this work and measured by the same method in our new laboratory in 2014 in Jena gave 45.2±1.2 $J \cdot g^{-1}$. The values overlap marginally within their uncertainties, the difference could be caused by the different samples. This is a difference of 0.53 $kJ \cdot mol^{-1}$, significantly less than the final uncertainty of > 2 $kJ \cdot mol^{-1}$ on the enthalpy of formation. For the results here, we adopt an arithmetic mean of all values (from 2006 and 2014) with the standard deviation of the mean of 15.23±0.22 $kJ \cdot mol^{-1}$ for the composition $(H_3O)_{1.34}Fe(SO_4)_{2.17}(H_2O)_{3.06}$ with molecular mass of 344.919 $g \cdot mol^{-1}$. With a properly constructed thermochemical cycle (Table 3), the enthalpy of formation of $(H_3O)_{1.34}Fe(SO_4)_{2.17}(H_2O)_{3.06}$ is calculated as –3202.1±2.6 $kJ \cdot mol^{-1}$.

The low-temperature heat capacity of rhomboclase was measured by relaxation calorimetry and is not a smoothly varying function. There is a distinct lambda-shaped anomaly with a maximum at T = 9.6 K (Fig. 3a). This anomaly corresponds very likely to a magnetic transition in rhomboclase. Because of the strong magnetic heat-capacity contribution at very low temperatures, we were not able to fit the C_p data with a Debye polynomial ($C_p = A_3T^3$). Instead, in the region below the transition (T < 15 K), the data were fit with an ordinary polynomial with the A_0 constant (in $C_p = A_0 + A_1T + A_2T^2 + \ldots$) set to zero. Care was taken to ensure that the polynomial does not plunge below 0 $J \cdot mol^{-1} \cdot K^{-1}$ in the region with no data (0-2 K).

Another broad anomaly is centered approximately at 180 K. This anomaly was detected by independent measurements of two different samples in comparable PPMS instruments in both Halifax and Salzburg, thus it is not sample- or instrument-related. We can only speculate about the nature of the increase and drop in heat capacity over a broad range of temperatures. The assumption of an onset of molecular motion in the H_5O_2 groups is most likely incorrect. Our models with high-frequency Einstein oscillators (results not shown) indicate that these do cause an increase in heat capacity but not its drop. Hence, they cannot reproduce such a broad anomaly under any conditions (frequency or number of such oscillators). A more likely reason for the anomaly is the melting of the adsorbed H_2O-H_2SO_4 mixture at the metastable eutectic point of water ice and sulfuric acid tetrahydrate at ~200 K (Gable et al. 1950).

The sample did not behave well in the PPMS calorimeter. First, the sample lost about 6.3 wt.% H_2O, although it was sealed in a crimped Al crucible. Perhaps more important,

Always consult and cite the final, published document. See http:/www.minsocam.org or GeoscienceWorld

the deviation between the PPMS and DSC data in the region of overlap (280-295 K) is unusually high, about 5 % (Fig. 3b). We have fitted two data sets and generated two standard entropy values for rhomboclase. One data set is based only on the PPMS data, for the other one the PPMS data were adjusted to the DSC data in the region of overlap. Using only the PPMS data, we obtain S^0(rhomboclase) = 435.6 $J \cdot mol^{-1} \cdot K^{-1}$. The PPMS data adjusted to the DSC data (shifted upwards) give S^0(rhomboclase) = 484.9 $J \cdot mol^{-1} \cdot K^{-1}$. Both of these values are calculated for the composition $(H_3O)_{1.34}Fe(SO_4)_{2.17}(H_2O)_{3.06}$ with molecular mass of 344.919 $g \cdot mol^{-1}$. Given the molecular mass and the nature (hydration state) of this phase, both of these values appear to be too high and deserve further attention.

Figure 4 shows the measured entropy for a number of Fe and Cu oxysalts (all data from our group, measured by PPMS) *versus* $-T(S_{measured}-S_{estimated})$. The variable plotted on the ordinate represents the contribution of the difference in the entropies to the Gibbs free energy. The estimates in Fig. 4 are based on the simple Kopp rule stating that the entropy of a phase is simply the sum of entropies of its components. For example, the estimated entropy for α-FeOOH (goethite) is the sum of entropies of $0.5S^0(\alpha\text{-}Fe_2O_3)$ and $0.5S^0(H_2O,solid)$. For $S^0(H_2O,solid)$, we have adopted the value of 41.94 $J \cdot mol^{-1} \cdot K^{-1}$ (Majzlan et al. 2003). For $S^0(SO_3,solid)$, the value of 63.85 $J \cdot mol^{-1} \cdot K^{-1}$ (Majzlan et al. 2015) was used. All other entropies for oxide components were taken for actual oxide phases from Robie and Hemingway (1995).

All $-T(S_{measured}-S_{estimated})$ data points fall into a range of ±7 $kJ \cdot mol^{-1}$, with exceptions that are relevant for this study. Both entropy values calculated for rhomboclase (shown by a square and a triangle in Fig. 4) deviate significantly from the rest of the data. The third data point that deviates is that of zýkaite, $Fe_4(AsO_4)_3(SO_4)(OH) \cdot 15H_2O$. This mineral is always poorly crystalline and the difference between the measured and estimated entropies can be easily explained by its poor crystallinity (Majzlan et al. 2015). Rhomboclase, however, possesses excellent crystallinity and there is no reason to expect the deviations seen in Fig. 4 for this mineral. Hence, we conclude that the experimental difficulties during the C_p measurements on rhomboclase preclude a calculation of an accurate and precise entropy for rhomboclase. For the purposes of this study, we revert to the estimated entropy of 380.1 $J \cdot mol^{-1} \cdot K^{-1}$ for all further calculations.

Always consult and cite the final, published document. See http:/www.minsocam.org or GeoscienceWorld

Phase $(H_3O)Fe(SO_4)_2$: No thermodynamic data for this phase were available prior to this work. This phase is a dehydration product of rhomboclase, with actual composition $(H_3O)_{1.34}Fe(SO_4)_{2.17}$. Inserting the heat of dissolution of this phase in 5 *N* HCl into an appropriate thermochemical cycle (Table 3) yields the enthalpy of formation of –2276.2±2.8 kJ·mol^{-1} for the composition $(H_3O)_{1.34}Fe(SO_4)_{2.17}$. Measurement of low-temperature heat capacity for this phase was impossible because of the difficulties with handling and the potential for damage for the instrument. An estimate of 251.8 J·mol^{-1}·K^{-1} for $(H_3O)_{1.34}Fe(SO_4)_{2.17}$ was obtained by subtracting the entropy for 3.06 H_2O molecules from the entropy of rhomboclase (above). The entropy of an H_2O molecule in a structure of a solid was taken to be equal to the entropy of hypothetical H_2O ice at T = 298.15 K. This entropy was calculated by Majzlan et al. (2003) as 41.94 J·mol^{-1}·K^{-1}. Thermodynamic data for this phase are also summarized in Table 5.

Mathematical programming analysis (MAP)

MAP is a method that brings calorimetric data and equilibrium observations into consonance, resulting in so-called internally consistent data sets. This method has been widely used for rock-forming silicates (e.g., Berman 1988) and we applied it recently to ambient-temperature equilibria of hydrates of sulfates of divalent metals (Grevel and Majzlan 2009, 2011). The basics of MAP were outlined there and will not be repeated here. The equilibrium observations exploited in this work are the reversals in temperature-relative air humidity (RH) space.

The two phases studied are related by a simple hydration-dehydration reaction

$$(H_3O)_{1.34}Fe(SO_4)_{2.17}(H_2O)_{3.06} = (H_3O)_{1.34}Fe(SO_4)_{2.17} + 3.06H_2O$$

Given that the solid phases are pure and do not change compositions with temperature, the equilibrium constant for this reaction is solely a function of water vapor fugacity. In practical terms, this variable is often measured or expressed as the relative humidity of the air (RH). The relative humidity as a function of temperature for this reaction was measured and tabulated by Xu et al. (2010).

The results of the optimization are summarized in Table 5 and graphically shown in Fig. 5. The optimization algorithm converged quickly at a solution which lies within the

Always consult and cite the final, published document. See http:/www.minsocam.org or GeoscienceWorld

uncertainties of the experimental data and satisfies the observations of Xu et al. (2010). This convergence supports the accuracy of the data obtained in our study, including our entropy estimates.

Solubility of rhomboclase and the Pitzer model for Fe(III)-SO_4 solutions

Solubility measurements have historically been a preferred way to derive thermodynamic data for many minerals. They are more precise than the calorimetric data and they only require routine equipment able to analyze chemical composition of aqueous solutions. On the other hand, they are prone to errors because of inherent assumptions about the activity of the ions in the solution, ion association in the solution, and often also the congruent nature of dissolution. This method has not been applied to the ferric sulfates, with the exception of jarosite (e.g., Baron and Palmer 1996), because of the previously lacking and now available but complicated activity-molality model for concentrated Fe(III)-SO_4 solutions.

The results of the calculation of solubility for rhomboclase are compared to the experimentally measured solubility in Fig. 6. The two curves correspond to two parametrizations of the Pitzer model by Tosca et al. (2007), one of them valid up to total molality of 3.0, the other up to total molality of 5.47. The calculated curves deviate strongly from the data obtained in our study as well as those of Wirth and Bakke (1914) and Baskerville and Cameron (1935). The model predicts significantly lower molalities of both $Fe_2(SO_4)_3$ and H_2SO_4 in solutions co-existing with rhomboclase.

To further examine the model and the available thermodynamic data, we used the data for the "basic" ferric sulfate hydronium jarosite, $(H_3O)Fe_3(SO_4)_2(OH)_6$. There are no data for aqueous solubility of hydronium jarosite at 25 ºC, but Posnjak and Merwin (1922) measured its solubility at 50 ºC. It can be assumed that the difference between the solubilities at these two temperatures is not very large for the purposes of a rough comparison. Thermodynamic data for hydronium jarosite were reported by Majzlan et al. (2004). They showed that the calculated solubility at 25 ºC corresponds roughly to the reported solubility at 50 ºC (Posnjak and Merwin 1922) at the lowest $Fe_2(SO_4)_3$ and H_2SO_4 molalities, at which simple activity-molality relations can be used. The results of solubility calculation for hydronium jarosite, using a simple activity-molality model

Always consult and cite the final, published document. See http:/www.minsocam.org or GeoscienceWorld

(Davies equation) and the more complex Pitzer model, are shown in Fig. S1 and discussed in the electronic annex. In short, the Davies equation, although not meant to be used at high ionic strengths, performs better than the Pitzer model.

Another reason for the failure for rhomboclase could lie in the estimated entropies. For reasons outlined above, we discarded the experimental entropies and used only estimates. The measured entropies, however, are too high and would make the disagreement seen in Fig. 6 only worse. The difference between Gibbs free energy for rhomboclase reported here and Gibbs free energy for rhomboclase needed for a perfect agreement between Pitzer model and experimental solubility is about 6 $kJ \cdot mol^{-1}$. If that difference is compensated by a shift in entropy (i.e., the experimental enthalpy is considered to be accurate), it would mean a shift of 20 $J \cdot mol^{-1} \cdot K^{-1}$, down to ~360 $J \cdot mol^{-1} \cdot K^{-1}$ for the standard entropy of rhomboclase. Such a shift would mean, however, that the entropy of rhomboclase would be a noticeable outlier, in this case too low and not supported by the systematics in Fig. 4. Thus, there are no arguments in favor for such a shift.

Crystal chemistry of rhomboclase and the mobility of hydrogen in its structure

Solid state ^2H MAS NMR spectra were recorded on deuterated rhomboclase $(D_5O_2)Fe(SO_4)(D_2O)_2$ to gain insight into the different deuterium species present in the mineral (Fig. 7). Rhomboclase contains two different local deuterium environments, a D_2O molecule directly coordinated to Fe(III), Fe-OD_2, and the $D_5O_2^+$ ion in the interlayer. The interpretation of the NMR spectra is based on our previous solid state ^2H NMR work on stoichiometric and defect jarosite minerals (Nielsen et al. 2008, 2011). There are two different deuterium resonances with isotropic chemical shifts $\delta_{iso}(^2H)$ = of 8±1 and 228±1 ppm, which constitute approximately 33 and 67 % of the total spectra intensity, respectively. The site with $\delta_{iso}(^2H)$ = 228 ppm has a significant paramagnetic shift, which shows this deuterium ion to be directly coordinated to Fe(III) via an oxygen, i.e., the Fe-OD_2 group in the structure, whereas the site with $\delta_{iso}(^2H)$ = of 8±1 has a negligible paramagnetic shift and originates from the $D_5O_2^+$ ion. This value resembles that observed for the H_3O^+ ion in jarosite (Nielsen et al. 2008). Further insight can be gained by analysis of the spinning side band manifold, which shows rapid rotation of the OD_2 group around the Fe-O bond vector at room temperature resulting in a quadrupole

Always consult and cite the final, published document. See http:/www.minsocam.org or GeoscienceWorld

coupling constants and asymmetry parameters of 100(20) kHz and 0.7(1), respectively. These values are very similar to those obtained for the Fe-OD_2 defects in jarosite (Nielsen et al. 2008). Only a single resonance is seen from the $D_5O_2^+$ ion, implying rapid molecular motion and possibly chemical exchange at room temperature making the five protons in the $D_5O_2^+$ unit indistinguishable on the NMR time scale. This is further supported by the smaller size of the quadrupole interaction ($C_Q \approx$ 40-50 kHz). The relative intensity of the Fe-OD_2 and $D_5O_2^+$ resonances of 30(3) and 70(4) %, respectively, deviate significantly from the expected 44 % and 66 % based on the formula $(H_5O_2)Fe(SO_4)_2 \cdot 2H_2O$. However, TGA results are in agreement with the presence of excess water in the interlayer of rhomboclase. TGA for deuterated rhomboclase shows two distinct mass losses in the region 50 to 270 °C and 630 to 720 °C corresponding to the conversion of rhomboclase to anhydrous iron(III) sulfate followed by formation of iron(III) oxide, respectively. However, the total mass loss for the first step (54 %) is larger than expected (39 %) based on a chemical formula for rhomboclase of $(D_5O_2)Fe(SO_4)_2(D_2O)$. The additional weight loss is equivalent to ~ 2.2 additional water molecules resulting in a formula of approximately $(D_5O_2)Fe(SO_4)_2(H_2O) \cdot 2.2D_2O$. With this composition, 30 % of the spectral intensity will be from the Fe-OD_2 groups, in excellent agreement with the intensities determined from analysis of the ^2H MAS NMR spectra.

Crystal chemistry of $(H_3O)Fe(SO_4)_2$ and the mobility of hydrogen in its structure

The initial structure for the molecular dynamic simulations with the exception of the hydronium ions was taken from our Rietveld refinement (see Fig. 8, Table 6). One H_3O^+ per $Fe(SO_4)_2$ was added to the structure for charge neutrality as a planar unit between the tetrahedral-octahedral sheets (Fig. 9a). The position of O in this H_3O^+ unit was (0,1/2,1/2), the initial O-H bond length 1.0 Å, and the H-O-H angles 120°. The initial hydronium orientation was such that one of the O-H bonds pointed in the *–b* direction. The second hydronium group in the unit cell was generated by shifting the first group with fixed orientation to a position with the central oxygen ion at (1/2, 0, 1/2). The supercell for the molecular dynamic simulations was obtained by doubling the cell parameter in the *a*-direction. Hence, the simulation supercell contained four H_3O^+ units.

Always consult and cite the final, published document. See http:/www.minsocam.org or GeoscienceWorld

A crystallographic information file (cif) is attached in an electronic annex to this publication. The file contains the information extracted from the powder XRD refinement and the *ab initio* calculation.

The *ab-initio* molecular dynamic simulations were performed at T = 300 K for 4.5 ps. The H_3O^+ groups did not dissociate but the initial planar H_3O^+ geometry evolved into a pyramidal structure (Fig. 9b), as expected. The time averages over the last 1 ps of the simulation for the O-H, O…O distances, the H-O-H, and O-H…O angles are, 1.025(23) Å, 2.69(11) Å, 112.6(1.0)°, 165.5(3.2)°, respectively. This bond geometry is in the experimentally observed range for other hydronium bearing compounds, such as $(H_3O)(HSO_4)$ with d(O-H) in the range of 0.85-0.93 Å and H-O-H angles between 102° and 118° (Kemnitz et al. 1996). The stability of the H_3O^+ groups is likely due to the strong covalent nature of the intramolecular O-H bonds as compared to the relatively weak O-H…O bonds that connect these groups to the tetrahedral-octahedral sheets.

Of the four H_3O^+ units in the simulation cell, two maintained their orientation throughout the calculation. One H_3O^+ rotated to a configuration where all three hydrogen atoms participate in hydrogen bonding. The fourth H_3O^+ molecule rotates independently of the other groups and adopts for the last ~1 ps of the run the same orientation as the third H_3O^+ molecule (Fig. 9c, 10). Once the configuration shown in Fig. 9c was attained, no further rotation of the H_3O^+ groups was observed. The final positions of the non-H atoms conformed to the –1 symmetry and are reported in Table 7. The positions of the H atoms are reported with a statistical 50 % occupancy because of the two possible orientations of each H_3O group. The structural model, obtained by a combination of Rietveld refinement and *ab-initio* calculation, is shown in Fig. 11.

In order to analyze the time dependence of the H_3O^+ ion geometry further, we determined the displacement of the oxygen parallel to the normal of the plane that is defined by the three hydrogen atoms of each H_3O^+ ion (hereafter the H_3 plane) (Fig. 12). We adopt the following sign convention: for a positive value of the displacement, the H_3 plane is above the oxygen ion and vice versa. For the final ~1 ps of the simulation we observe that the sign of the displacements does not change with the exception of a few short lived excursions (less than 0.2 ps). Since the planes for each H_3O^+ ion are

Always consult and cite the final, published document. See http:/www.minsocam.org or GeoscienceWorld

subparallel to the (001) plane this finding implies that it is unlikely that the time averaged crystallographic positions of hydrogen ions show z=0.5.

Relaxing the structure at 0 K shows that the hydronium arrangement that we found in the MD simulations (Fig. 9c) is ~0.4 eV per $(H_3O)Fe(SO_4)_2$ more stable than the initial arrangement with the planar H_3O^+ groups (Fig. 9a). The average Fe-O and S-O bond length are 2.009(14) Å and 1.485(6) Å. The hydrogen bond scheme remains unaltered with respect to the *ab-initio* molecular dynamics simulations. The average O-H bond distance of the H_3O^+ units is 1.025(23) Å and the average H-O-H angle is 112.6(1.0)°. We also find that the H_3O^+ units are tilted off the [011] direction by a small angle of 3.9(1)°. The average O…H, and O…O distances and the H-O-H, and O-H…O angles are 1.020(21) Å, 2.68(12) Å, 112.4(1.2)°, and 174.9(2.9)°, respectively.

During the *ab-initio* molecular dynamics simulations not all thermodynamically accessible structures may have been probed. There may exist configurations on much longer timescales than those accessible in our molecular dynamics simulations. In order to test this possibility, we explored the energetics of hydronium motion (translation and rotation) in one unit cell (30 atoms) further using constrained static calculations. In all calculations, displacements/rotations have only been applied to one H_3O^+ unit and the unit cell as well as remaining atomic positions were fixed at the values obtained from the static relaxation. Thus, the calculated energies are likely the upper bounds for dynamic rearrangements of the structure. We find that the rotation of the H_3O^+ groups around an axis normal to the H_3 plane is significantly hindered (Fig. 13). The barriers are 56 meV/3 H atoms, corresponding to ~650 K and it is unlikely that the hydronium units can rotate freely at ambient temperature. Our static calculations corroborate our *ab-initio* molecular dynamics simulation in that pure rotational disorder due to different orientations of the H_3O^+ units is unlikely. We also considered two translational types of motion (Fig. 14): displacement of a complete H_3O^+ group along the vector *N* (Fig. 14, inset) normal to the H_3 plane and displacement of the hydrogen atoms only for a fixed oxygen position. For the first case, we find that the energy required to move a H_3O^+ ion is small compared to the thermal energy provided at 300 K since only the relatively weak hydrogen bonds are affected. In particular, the oxygen atoms of the H_3O^+ groups are shifted by ≤0.04 Å off the *z*=1/2 plane. For the second case, we found that the motion is much more restricted

Always consult and cite the final, published document. See http:/www.minsocam.org or GeoscienceWorld

and it is unlikely that the H_3 can switch from below to above the central oxygen ion or vice versa. In particular, we found only one energy minimum for this type of motion. This finding can be rationalized by realizing that that this motion leads to a H_3O^+ geometry that is almost an exact mirror image of the initial geometry (the mirror plane is subparallel to the (001)-plane). In the final configuration hydrogen bonding is much weaker as compared to the initial geometry since the O-H bonds do not point towards oxygens of the SO_4 tetrahedra but in a direction that is sub-parallel to the bisector of O(S)…O(H_3O^+)…O(S) angle.

The *ab-initio* molecular dynamics simulations and the static simulations show that the H_3O^+ ions may exhibit different types of motion. Translating (shifting) the entire hydronium group requires only a comparatively small energy. On the other hand, rotational motion of the hydronium ions appears to be significantly hindered. Similarly, translating the hydrogen atoms of a hydronium group is restricted. The two latter types of motion are difficult to carry out because they involve breaking of several hydrogen bonds; this could be possible only if the temperature was elevated to ~650 K or above. It is interesting to compare our calculations to NMR observations (Yaroslavtsev et al. 1983) on $(H_3O)In(SO_4)_2$ and $(H_3O)Tl(SO_4)_2$. They found that the H_3O^+ groups do not rotate at all at liquid nitrogen temperature in $(H_3O)Tl(SO_4)_2$. In $(H_3O)In(SO_4)_2$, motion of these groups could be detected even at the liquid nitrogen temperature. At T = 220 K, 60-80 % of the H_3O^+ groups rotate and the fraction of the rotating groups further increases with increasing temperature.

The hydrogen bonding scheme obtained by the molecular dynamics simulation indicates that the hydronium ions orient themselves such that they provide hydrogen bonding to each non-bridging oxygen of the sulfate tetrahedra. Thus, our static results indicate that the likely time-averaged symmetry is $P1$ rather than $P\bar{1}$ due to the presence of the H_3O^+ ions. A similar conclusion was drawn for $(H_3O)Tl(SO_4)_2$ by Yaroslavtsev et al. (1983). However, we cannot exclude the existence of two or more states that are energetically nearly degenerate with the groundstate we found and related by correlated motion of at least two H_3O^+ molecules. This may allow to restore the $P\bar{1}$ symmetry as long time averages. Nevertheless our findings suggest that at least the low-temperature

Always consult and cite the final, published document. See http:/www.minsocam.org or GeoscienceWorld

634 groundstate of $(H_3O)Fe(SO_4)_2$ is triclinic without inversion symmetry, if the positions of
635 the H atoms are taken into account.

636 ## IMPLICATIONS

637 Our results have implications for the geochemical modeling of AMD systems. They
638 show that within the experimental constraints (measured and estimated thermodynamic
639 functions, brackets in temperature-relative humidity space, solubility data), it is so far not
640 possible to obtain an internally consistent thermodynamic model for rhomboclase and co-
641 existing aqueous solutions. More work is needed to identify the sources of the
642 discrepancies if geochemical models of AMD systems based on equilibrium
643 thermodynamic data for ferric sulfates are to be fully trusted.

644 **Acknowledgements**. We thank two anonymous reviewers for their constructive
645 comments. We are thankful to Tina Block and Artur Banaszewski for the sample
646 preparation. This project was financially supported by a *Deutsche*
647 *Forschungsgemeinschaft* (DFG) grant MA 3927/21-1. We acknowledge the ANKA
648 Angströmquelle Karlsruhe for the provision of the beamtime at the PDIFF beamline and
649 Stephen Doyle for the support during the measurements at the beamline. UGN
650 acknowledges the Villum Foundation for a "Villum Young Investigator Programme"
651 (grants VKR022364). EG is grateful for financial support from Oticon Fonden. We
652 acknowledge the support of the Canada Foundation for Innovation, the Atlantic
653 Innovation Fund, and other partners which fund the Facilities for Materials
654 Characterization, managed by the Institute for Research in Materials.

655 ## REFERENCES

656 Anawar, H. (2015) Sustainable rehabilitation of mining waste and acid mine drainage using
657 geochemistry, mine type, mineralogy, texture, ore extraction and climate knowledge. Journal
658 of Environmental Management, 158, 111–121.
659 Appleby, M.P., and Wilkes, S.H. (1922) The system ferric oxide - sulfuric acid - water. Journal of
660 the Chemical Society, 21, 337–348.
661 Baron, D., and Palmer, C.D. (1996) Solubility of jarosite at 4–35 ºC. Geochimica et
662 Cosmochimica Acta, 60, 185–195.
663 Baskerville, W. H., and Cameron, F.K. (1935) Ferric oxide and aqueous sulfuric acid at 25 ºC.
664 Journal of Physical Chemistry, 39, 769–779.
665 Berman, R.G. (1988) Internally-consistent thermodynamic data for minerals in the system Na_2O-
666 K_2O-CaO-MgO-FeO-Fe_2O_3-Al_2O_3-SiO_2-TiO_2-H_2O-CO_2. Journal of Petrology, 29, 445-522.
667 Bigham, J.M., Schwertmann, U., and Pfab, G. (1996) Influence of pH on mineral speciation in a
668 bioreactor simulating acid mine drainage. Applied Geochemistry, 11, 845–849.
669 Blöchl, P.E. (1994) Projector augmented-wave method. Physical Review B, 50, 17953–17979.

Always consult and cite the final, published document. See http:/www.minsocam.org or GeoscienceWorld

Blowes, D.W., Ptacek, C.J., Jambor, J.L., and Weisener, C.G. (2003) The geochemistry of acid mine drainage. Treatise on geochemistry, Volume 9. Editor: Barbara Sherwood Lollar. Executive Editors: Heinrich D. Holland and Karl K. Turekian. Elsevier, p.149–204.

Bolanz, R.M., Göttlicher, J., Steininger, R., Wieczorek, A. 2016: Structural incorporation of As^{5+} into rhomboclase ($(H_5O_2)Fe^{3+}(SO_4)_2 \cdot 2H_2O$) and $(H_3O)Fe(SO_4)_2$. Chemosphere, 146, 338-345.

Brach, I., and Goodenough, J.B. (1988) Influence of the M(III) cation on proton conduction in rhomboclases. Solid State Ionics, 27, 243–249.

Buckby, T., Black, S., Coleman, M.L., and Hodson, M.E. (2003) Fe-sulphate-rich evaporative mineral precipitates from the Rio Tinto, southwest Spain. Mineralogical Magazine, 67, 263–278.

Byrne, P., Wood, P.J., and Reid, I. (2012) The impairment of river systems by metal mine contamination: A review including remediation options. Critical Reviews in Environmental Science and Technology, 42, 2017–2077.

Cameron, F.K., and Robinson, C. (1907) Ferric sulphates. Journal of Physical Chemistry, 11, 641–650.

Chase, M.W., Jr. (1998) NIST-JANAF Thermochemical Tables. Fourth Edition. Journal of Physical Chemistry Reference Data, Monograph no. 9, 1538.

DeKock, C.W. (1982) Thermodynamic properties of selected transition metal sulfates and their hydrates. U.S. Bureau of Mines Information Circular, 8910, 45p.

DeKock, C.W. (1986) Thermodynamic properties of selected metal sulfates and their hydrates. U.S. Bureau of Mines Information Circular, 9081, 59p.

Gable, C.M., Betz, H.F., and Maron, S.H. (1950) Phase equilibria of the system sulphur trioxide-water. Journal of the American Chemical Society, 72, 1445–1448.

Garris, H.W., Baldwin, S.A., and Van Hamme, J.D. (2016) Genomics to assist mine reclamation: a review. Restoration Ecology, 24, 165–173.

Grevel, K.-D., and Majzlan, J. (2009) Internally consistent thermodynamic data for magnesium sulfate hydrates. Geochimica et Cosmochimica Acta, 73, 6805–6815.

Grevel, K.-D., and Majzlan, J. (2011) Internally consistent thermodynamic data for metal divalent sulphate hydrates. Chemical Geology, 286, 301–306. Doi:10.1016/j.chemgeo.2011.05.016

Hallberg, K.B. (2010) New perspectives in acid mine drainage microbiology. Hydrometallurgy, 104, 448–453.

Hamann, D.R. (1997) H_2O hydrogen bonding in density-functional theory. Physical Review B, 55, 10157–10160.

Hohenberg, P., and Kohn, W. (1964) Inhomogeneous electron gas. Physical Review B, 136, 864–871.

Holzwarth, N.A.W., Matthews, G.E., Dunning, R.B., Tackett, A.R., and Zeng, Y. (1997) Comparison of the projector augmented-wave, pseudopotential, and linearized augmented-plane-wave formalisms for density-functional calculations of solids. Physical Review B, 55, 2005–2017.

Jerz, J.K., and Rimstidt, J.D. (2003) Efflorescent iron sulfate minerals: Paragenesis, relative stability, and environmental impact. American Mineralogist, 88, 1919–1932.

Johnson, D.B., and Hallberg, K.B. (2005) Acid mine drainage remediation options: a review. Science of Total Environment, 338, 3–14.

Kemnitz, E., Werner, C., and Troyanov, S.I. (1996) Reinvestigation of crystalline sulfuric acid and oxonium hydrogensulfate. Acta Crystallographica, C52, 2665–2668.

Kennedy, C.A., Stancescu, M., Marriott, R.A., and White, M.A. (2007) Recommendations for accurate heat capacity measurements using a Quantum Design physical property measurement system. Cryogenics, 47, 107–112.

Klein, R., Tischler, J. S., Muehling, M., Schlömann, M. (2014) Bioremediation of mine water. Edited by: Schippers, A., Glombitza, F., Sand, W. Geobiotechnology I: Metal-related issues. Advances in Biochemical Engineering-Biotechnology, 141, 109–172.

Always consult and cite the final, published document. See http:/www.minsocam.org or GeoscienceWorld

Koerker, F.W., Calderwood, H.H. (1938) The system ferric oxide-sulfur trioxide-water. Journal of Physical Chemistry, 42, 1151–1155.

Kohn, W., and Sham, L.J. (1965) Self-consistent equations including exchange and correlation effects. Physical Review A, 140, 1133–1138.

Kresse, G., and Joubert, D. (1999) From ultrasoft pseudopotentials to the projector augmented-wave method. Physical Review B, 59, 1758–1775.

Kresse, G., and Hafner, J. (1993) *Ab-initio* molecular dynamics of liquid metals. Physical Review B, 47, RC 558–561.

Kresse, G., and Furthmüller, J. (1996a) Efficiency of *ab-initio* total-energy calculations using a plane-wave basis set. Computational Materials Sciences, 6, 15–50.

Kresse, G., and Furthmüller, J. (1996b) Efficient iterative schemes for *ab-initio* total-energy calculations using a plane-wave basis set. Physical Review B, 54, 11169–11186.

Lacey, D.T., and Lawson, F. (1970) Kinetics of the liquid-phase oxidation of acid ferrous sulfate by the bacterium *Thiobacillus ferrooxidans*. Biotechnology and Bioengineering, 12, 29–50.

Larson, A.C., and von Dreele, R.B. (1994) *GSAS. General Structure Analysis System*. LANSCE, MS-H805, Los Alamos, New Mexico.

Lemire, R.J., Berner, U., Musikas, C., Palmer, D.A., Taylor, P., and Tochiyama, O. (2013) Chemical Thermodynamics of Iron. Nuclear Energy Agency, OECD, Elsevier.

Majzlan, J., Grevel, K.-D., and Navrotsky, A. (2003) Thermodynamics of iron oxides: Part II. Enthalpies of formation and relative stability of goethite (α-FeOOH), lepidocrocite (γ-FeOOH), and maghemite (γ-Fe_2O_3). American Mineralogist, 88, 855–859.

Majzlan, J., Navrotsky, A., McCleskey, R.B., and Alpers, C.N. (2006) Thermodynamic properties and crystal structure refinement of ferricopiapite, coquimbite, rhomboclase, and $Fe_2(SO_4)_3(H_2O)_5$. European Journal of Mineralogy, 18, 175–186.

Majzlan, J., Navrotsky, A., Stevens, R., Donaldson, M., Woodfield, B.F., and Boerio-Goates, J. (2005) Thermodynamics of monoclinic $Fe_2(SO_4)_3$. Journal of Chemical Thermodynamics, 37, 802–809.

Majzlan, J., Amoako, F.Y., Kindlová, H., and Drahota, P. (2015) Thermodynamic properties of zýkaite, a ferric sulfoarsenate. Applied Geochemistry, 61, 294–301.

Majzlan, J., Stevens, R., Boerio-Goates, J., Woodfield, B.F., Navrotsky, A., Crawford, M., Burns, P., and Amos, T.G. (2004) Thermodynamic properties, low-temperature heat capacity anomalies, and single crystal X-ray refinement of hydronium jarosite, $(H_3O)Fe_3(SO_4)_2(OH)_6$. Physics and Chemistry of Minerals, 31, 518–531.

Mereiter, K. (1974) Die Kristallstruktur von Rhomboklas, $(H_5O_2)^+(Fe(SO_4)_2(H_2O)_2)$. Tschermaks Mineralogische und Petrologische Mitteilungen, 21, 216–232.

Merwin, H.E., and Posnjak, E. (1937) Sulphate incrustations in the copper Queen mine, Bisbee, Arizona. American Mineralogist, 22, 567–571.

Mookherjee, M., and Stixrude, L. (2006) High pressure proton disorder in brucite. American Mineralogist, 91, 127–134.

Nielsen, U.G., Heinmaa, I., Samoson, A., Majzlan, J., and Grey, C.P. (2011) Insight into the local magnetic environments and deuteron mobility in jarosite ($AFe_3(SO_4)_2(OD,OD_2)_6$, A = K, Na, D_3O) and hydronium alunite ($(D_3O)Al_3(SO_4)_2(OD)_6$), from variable temperature ^2H MAS NMR spectroscopy. Chemistry of Materials, 23, 3176–3187. Doi 10.1021/cm2003929

Nielsen, U.G., Majzlan, J., and Grey, C.P. (2008) Determination and quantification of the local environments in stoichiometric and defect jarosite by solid-state ^2H NMR spectroscopy. Chemistry of Materials, 20, 2234–2241, Doi 10.1021/cm702523d

Nordstrom, D.K. (1982) Aqueous pyrite oxidation and the consequent formation of secondary iron minerals. In: Kittrick, J.A., Fanning, D.S., and Hosner, L.R. (eds), Acid sulfate weathering, Soil Science Society of America, Madison, Wisconsin, 37–56.

Always consult and cite the final, published document. See http:/www.minsocam.org or GeoscienceWorld

Nordstrom, D.K., and Southam, G. (1997) Geomicrobiology of sulfide mineral oxidation. In: Banfield, J.F., and Nealson, K.H. (eds), Geomicrobiology: interactions between microbes and minerals, vol. 35. Mineralogical Society of America, Washington, DC, 361–390.

Nordstrom, D.K., Alpers, C.N., Ptacek, C.J., and Blowes, D.W. (2000) Negative pH and extremely acidic mine waters from Iron Mountain, California. Environmental Science and Technology, 34, 254–258.

Nosé, S. (1984) A unified formulation of the constant temperature molecular-dynamics methods. Journal of Chemical Physics, 81, 511–519.

Parbhakar-Fox, A., and Lottermoser, B.G. (2015) A critical review of acid rock drainage prediction methods and practices. Minerals Engineering, 82, 107–124.

Parker, V.B. (1965) Thermal properties of uni-univalent electrolytes. National Standard Reference Data Series, National Bureau of Standards, 2, 66 pp.

Parkhurst, D.L., and Appelo, C.A.J. (1999) User's guide to PHREEQC (Version 2) -a computer program for speciation, batch-reaction, one-dimensional transport, and inverse geochemical calculations. USGS Water-Resources Investigations Report, 99–4259, 312 pp.

Perdew, J.P., Burke, K., and Ernzerhof, M. (1996) Generalized gradient approach made simple. Physical Review Letters, 77, 3865–3868.

Perkins, E.H., Nesbitt, H.W., Gunter, W.D., St-Arnaud, L.C., and Mycroft, J.R. (1995) Critical review of geochemical processes and geochemical models adaptable for prediction of acidic drainage from waste rock. Mine Environment Neutral Drainage (MEND) Program Prediction Committee, 283 pp.

Peterson, R.C., Valyashko, E., and Wang, R.Y. (2009) The atomic structure of $(H_3O)Fe^{3+}(SO_4)_2$ and rhomboclase, $(H_5O_2)Fe^{3+}(SO_4)_2{\cdot}2H_2O$. Canadian Mineralogist, 47, 625–634.

Posnjak, E., and Merwin, H.E. (1922) The system, $Fe_2O_3 – SO_3 – H_2O$. Journal of the American Chemical Society, 44, 1965–1994.

Recoura, P. (1907) Recherches sur le sulfate ferrique. Annales de chimie et de physique, 11, 263–288.

Robie, R.A., Hemingway, B.S. (1995. Thermodynamic properties of minerals and related substances at 298.15 K and 1 bar (105 Pascals) and at higher temperatures. U.S. Geological Survey Bulletin, 2131, IV + 461 p.

Sejkora, J., Malíková, R., and Novák, M. (2015) Alteration products from experiments of controlled alteration of pyrite and marcasite. Bulletin mineralogicko-petrologického oddělení Národního muzea v Praze, 23 (2), 261–270. (in Czech, with English abstract)

Sheoran, A.S., and Sheoran, V. (2006) Heavy metal removal mechanism of acid mine drainage in wetlands: A critical review. Minerals Engineering, 19, 105–116.

Stoffregen, R.E. (1993) Stability relations of jarosite and natrojarosite at 150-250 ºC. Geochimica et Cosmochimica Acta, 57, 2417–2429.

Tosca, N.J., Smirnov, A., and McLennan, S.M. (2007) Application of the Pitzer ion interaction model to isopiestic data for the $Fe_2(SO_4)_3$-H_2SO_4-H_2O system at 298.15 and 323.15 K. Geochimica et Cosmochimica Acta, 71, 2680–2698.

Tsuchiya, J., Tsuchiya, T., and Tsuneyuki, S. (2005) First-principles study of hydrogen bond symmetrization of phase D under high pressure. American Mineralogist, 90, 44–49.

Wirth, F., and Bakke, B. (1914) Untersuchung über Ferrisulfate. Darstellung und Eigenschaften der verschiedenen normalen, basischen und sauren Ferrisulfate. Löslichkeits- und Stabilitätsverhältnisse in Wasser und Schwefelsäure. Kristallisationsgang. Zeitschrift für anorganische Chemie, 87, 13–46.

Yaroslavtsev, A.B., Prozorovskaya, Z.N., Tschuvayev, V.F., and Spicyn, V.I. (1983) Mobility of oxonium ions in indium and thallium acid sulfate monohydrates. Zhurnal Neorganicheskoi Khimii, 28, 2495–2498.

Xu, W., Parise, J., and Hanson, J. (2010) $(H_3O)Fe(SO_4)_2$ formed by dehydrating rhomboclase and its potential existence on Mars. American Mineralogist, 95, 1408–1412.

Always consult and cite the final, published document. See http:/www.minsocam.org or GeoscienceWorld

TABLE 1. Chemical composition of the solutions equilibrated with rhomboclase. All data in wt.% determined by ICP-OES. Molalities of the two components were calculated from the wt.% data.

Charge	SO_3 wt.%	Fe_2O_3 wt.%	$Fe_2(SO_4)_3$ molality	H_2SO_4 molality
room temperature				
TB-22	33.10	6.163	0.6970	5.376
TB-23	33.15	6.136	0.6943	5.398
TB-25	33.31	5.140	0.5769	5.726
TB-26	33.52	4.794	0.5383	5.894
TB-27	34.47	3.088	0.3469	6.683
TB-28	35.13	2.344	0.2648	7.122
TB-29	36.80	1.172	0.1355	8.082
TB-30	38.18	0.5795	0.06867	8.820
temperature 4 ºC				
TB23-K	29.73	5.434	0.5672	4.487
TB25-K	29.91	4.101	0.4235	4.891
TB27-K	31.07	2.372	0.2460	5.691
TB29-K	33.14	0.8469	0.09014	6.766

TABLE 2. Lattice parameters (Å), unit-cell volume ($Å^3$), and fractional coordinates of the interlayer O atom (x, 0.25, z) refined from synchrotron powder XRD patterns of rhomboclase samples synthesized from solutions with variable H_2SO_4 molarity (M).

Sample	M	*a*	*b*	*c*	*V*	*x*	*z*
AB1	2.71	9.7222(1)	18.2833(3)	5.42618(6)	964.52(2)	0.388(1)	0.574(3)
AB6	2.71	9.7221(1)	18.2856(1)	5.42618(4)	964.63(1)	0.389(1)	0.573(2)
AB7	3.38	9.7213(1)	18.2838(3)	5.42573(6)	964.38(2)	0.391(2)	0.571(3)
AB8	3.93	9.7228(1)	18.2862(2)	5.42681(6)	964.85(2)	0.389(2)	0.571(3)

Always consult and cite the final, published document. See http:/www.minsocam.org or GeoscienceWorld

TABLE 3A. Thermochemical cycle for the studied compounds. All reactants and products at T = 298.15 K and P = 1 bar. Abbreviations: cr = crystalline solid; l = liquid; aq = aqueous species; g = gas.

reaction number and reaction
1 $MgO\ (cr) + 2H^+\ (aq) = Mg^{2+}\ (aq) + H_2O\ (aq)$
2 $\gamma\text{-}FeOOH{\cdot}0.162H_2O\ (cr) + 3H^+\ (aq) = Fe^{3+}\ (aq) + 2.162H_2O\ (aq)$
3 $\alpha\text{-}MgSO_4\ (cr) = Mg^{2+}\ (aq) + SO_4^{2-}\ (aq)$
4 $H_2O\ (l) = H_2O\ (aq)$
5 $\gamma\text{-}FeOOH{\cdot}0.162H_2O\ (cr) = \gamma\text{-}FeOOH\ (cr) + 0.162H_2O\ (l)$
6 $(H_3O)_{1.34}Fe(SO_4)_{2.17}{\cdot}nH_2O = Fe^{3+}\ (aq) + 2.17SO_4^{2-}\ (aq) + 1.34H^+\ (aq) + (n+1.34)H_2O\ (aq)$
7 $Fe\ (cr) + O_2\ (g) + 1/2H_2\ (g) = \gamma\text{-}FeOOH\ (cr)$
8 $H_2\ (g) + 1/2O_2\ (g) = H_2O\ (l)$
9 $Mg\ (cr) + 1/2O_2\ (g) = MgO\ (cr)$
10 $Mg\ (cr) + S\ (cr) + 2O_2\ (g) = \alpha\text{-}MgSO_4\ (cr)$
11 $Fe\ (cr) + 2.17S\ (cr) + (5.01+n/2)O_2\ (g) + (2.01+n)H_2\ (g) = (H_3O)_{1.34}Fe(SO_4)_{2.17}{\cdot}nH_2O\ (cr)$
$\Delta_fH^0\ [(H_3O)_{1.34}Fe(SO_4)_{2.17}{\cdot}nH_2O] = -2.17\Delta H_1 + \Delta H_2 + 2.17\Delta H_3 + (1.51+n)\Delta H_4 - \Delta H_5 - \Delta H_6 + \Delta H_7 + (1.51+n)\Delta H_8 - 2.17\Delta H_9 + 2.17\Delta H_{10}$

TABLE 3B. Enthalpy values for reactions listed in Table 3a. All values in $kJ{\cdot}mol^{-1}$. The values for reaction 6 are given separately for rhomboclase (reaction 6R) and $(H_3O)_{1.34}Fe(SO_4)_{2.17}$ (reaction 6A).

$\Delta H_1 = -149.68\pm0.60$ (9) (Majzlan et al. 2015 and references therein)
$\Delta H_2 = -46.62\pm0.13$ (12) (Majzlan et al. 2015 and references therein)
$\Delta H_3 = -53.50\pm0.48$ (7) (Majzlan et al. 2015 and references therein)
$\Delta H_4 = -0.54$ (calculated from Parker 1965)
$\Delta H_5 = 1.41\pm0.17$ (Majzlan et al. 2015 and references therein)
$\Delta H_{6R} = 15.23\pm0.22$ (10) (this work)
$\Delta H_{6A} = -38.05\pm1.16$ (2) (this work)
$\Delta H_7 = -549.4\pm1.4$ (Majzlan et al. 2003)
$\Delta H_8 = -285.8\pm0.1$ (Robie and Hemingway 1995)
$\Delta H_9 = -601.6\pm0.3$ (Robie and Hemingway 1995)
$\Delta H_{10} = -1288.8\pm0.5$ (DeKock 1986)

Always consult and cite the final, published document. See http:/www.minsocam.org or GeoscienceWorld

TABLE 4. Enthalpies of dissolution in 5 N HCl ($\Delta_{diss}H$) and enthalpies of formation (Δ_fH^o) for Ca and Mg oxides and sulfates. These data were collected in order to test the accuracy of the calorimetric data. All values in kJ·mol^{-1}. For details, see text. RH95 – Robie and Hemingway (1995), JANAF 1998 – Chase (1998).

	$\Delta_{diss}H$	Δ_fH^o	Δ_fH^o
CaO	–195.86±1.64	–635.1±0.9 (RH95)	–635.09±0.88 (JANAF 1998)
$CaSO_4$	10.76±0.21	–1434.4±4.2 (RH95)	–1433.8±3.20 (JANAF 1998)
MgO	–149.69±0.60	–601.6±0.3 (RH95)	–601.241±0.63 (JANAF 1998)
$MgSO_4$	–53.50±0.48	–1288.8±0.5 (DeKock 1986)	

TABLE 5. Results of the MAP optimization of thermodynamic functions for rhomboclase $[(H_3O)_{1.34}Fe(SO_4)_{2.17}(H_2O)_{3.06}]$ and $(H_3O)_{1.34}Fe(SO_4)_{2.17}$. Enthalpy values in kJ·mol^{-1}, entropy values in J·mol^{-1}·K^{-1}.

	initial value	value after optimization	difference
Δ_fH^0(rhomboclase)	–3202.08	–3202.03	0.05
S^0(rhomboclase)	380.1	378.7	–1.4
$\Delta_fH^0[(H_3O)_{1.34}Fe(SO_4)_{2.17}]$	–2276.20	–2276.25	–0.05
$S^0[(H_3O)_{1.34}Fe(SO_4)_{2.17}]$	251.8	253.2	1.4

TABLE 6. Crystallographic data for $(H_3O)Fe(SO_4)_2$ from Rietveld refinement and ab-initio calculations. Statistics of the Rietveld refinement with the rigid bodies in the model is given in the bottom portion of the table.

lattice parameters (Å, º)	Rietveld refinement	theory at constant experimental volume
a	4.8087(1)	4.803
b	8.3180(1)	8.404
c	8.3034(1)	8.218
α	70.181(1)	70.37
β	90.276(1)	90.25
γ	89.993(1)	90.22
V (Å^3)	312.44(1)	312.44
calculated density (g cm^{-3})	2.87	
number of data points	17747	
Le Bail χ^2	6.68	
Rietveld refinement with rigid bodies		
χ^2	9.73	
wR_p (fitted)	0.046	
R_p (fitted)	0.030	
wR_p (-background)	0.074	
R_p (-background)	0.054	

Always consult and cite the final, published document. See http:/www.minsocam.org or GeoscienceWorld

TABLE 7. Fractional atomic coordinates for $(H_3O)Fe(SO_4)_2$ obtained from the synchrotron powder XRD data, *ab-initio* calculations, and molecular dynamics simulation (see text for details). Space group is *P*–1 and the lattice parameters equal to those obtained from static calculations (see Table 6).

atom	*x*	*y*	*z*	*SOF*
Fe1	0	0	0	
Fe2	1/2	1/2	0	
S1	0.9887	0.2656	0.2129	
S2	0.5027	0.7539	0.2147	
O1	0.9633	0.2063	0.4056	
O2	0.1712	0.4170	0.1609	
O3	0.7004	0.3053	0.1436	
O4	0.1042	0.1243	0.1653	
O5	0.5219	0.6844	0.4062	
O6	0.6760	0.9093	0.1542	
O7	0.2105	0.7940	0.1640	
O8	0.6155	0.6199	0.1502	
O9	0	1/2	1/2	
O10	1/2	0	1/2	
H1	0.1545	0.5579	0.4772	0.5
H2	0.7947	0.5713	0.4650	0.5
H3	0.9705	0.3862	0.4710	0.5
H4	0.7148	0.0880	0.4628	0.5
H5	0.3545	0.0644	0.4807	0.5
H6	0.5427	0.8973	0.4744	0.5

Always consult and cite the final, published document. See http:/www.minsocam.org or GeoscienceWorld

FIGURE CAPTIONS

FIGURE 1. Back-scattered electron images of the rhomboclase sample used for calorimetry in this study. The droplets on the crystals are the result of outgassing in vacuum of the scanning electron microscope.

FIGURE 2. Solubility of ferric sulfates plotted in a H_2O-Fe_2O_3-SO_3 diagram. All symbols show the compositions of aqueous phases that co-existed with crystalline ferric sulfates. Circles – this study, room temperature; diamonds – this study, 4 ºC; triangles – Posnjak and Merwin (1922); squares – Baskerville and Cameron (1935); crosses – Wirth and Bakke (1914). Shaded symbols are for the samples where the co-existing solid was rhomboclase.

FIGURE 3. a) Low-temperature heat capacity data for rhomboclase, showing the magnetic transition in this phase. b) Difference between the relaxation calorimetry (PPMS) and differential scanning calorimetry (DSC) measurements for the rhomboclase sample.

FIGURE 4. The deviations of the standard entropies for a suite of ferric iron (small circles) and copper (small diamonds) oxysalts from the estimated entropies. The large square represents the calculated entropy for rhomboclase from the PPMS data, the large triangle the entropy calculated from the PPMS data adjusted to match the DSC data. The data point for zýkaite (marked in the figure) is also discussed in the text.

FIGURE 5. The result of the MAP analysis is shown by the a line that represents the calculated equilibrium curve for the hydration-dehydration reaction between rhomboclase and the phase $(H_3O)Fe(SO_4)_2$. The triangles show the brackets measured by Xu et al. (2010). Their data lie in the tips of the triangles, not in their centers.

FIGURE 6. Experimental (symbols) and calculated (curves) solubility of several ferric sulfates. Circles – this study, room temperature; squares – Baskerville and Cameron (1935), room temperature; crosses – Wirth and Bakke (1914), room temperature. Charges which precipitated rhomboclase are shown with grey symbols. Solubility curves for rhomboclase (marked R) and hydronium jarosite (marked J) were calculated with the Pitzer model of Tosca et al. (2007).

FIGURE 7. ^2H MAS NMR spectrum of rhomboclase with an expansion of the region for the isotropic shifts (inset).

FIGURE 8. Synchrotron X-ray diffraction pattern of $(H_3O)Fe(SO_4)_2$ with the calculated and difference plot from Rietveld refinement. The structural model used in this Rietveld refinement included rigid bodies (see text for details). The statistics of this refinement is listed in Table 6.

FIGURE 9. Orientation of the H_3O^+ groups in the interlayer space in the structure of $(H_3O)Fe(SO_4)_2$. a) initial model for the ab-initio calculations with planar H_3O^+ ions; b) early change of the H_3O^+ geometry from planar to pyramidal; c) the final orientation of the H_3O^+ groups after the MD simulation run. Note the change in orientation of two of the H_3O^+ groups.

FIGURE 10. Time evolution of the orientation of the H_3O^+ groups in the *ab-initio* molecular dynamics simulations. Shown are the angles after orthogonal projection of the hydronium groups in the (a,b)-plane (0° = +a-axis; 90° = +b-axis; –90° = –b-axis; ±180° = –a-axis).

FIGURE 11. Fully relaxed geometry of $(H_3O)Fe(SO_4)_2$ as obtained from the Rietveld refinement and subsequent *ab-initio* calculations and molecular dynamics simulation.

Always consult and cite the final, published document. See http:/www.minsocam.org or GeoscienceWorld

The octahedra house Fe, tetrahedra S. The hydronium ions are located in the interlayer portion of the structure. Note the tilt of the sulfate tetrahedra out of the *ab* plane and the alternating orientation of the hydronium ions to the upper and lower tetrahedral-octahedral layer. The dashed lines represent hydrogen bonds.

FIGURE 12. Time evolution of the distance between the oxygen atom from the H_3 plane in the H_3O^+ group from *ab-initio* molecular dynamics simulations. Negative (positive) values mean that the H_3 plane is below (above) the oxygen ion.

FIGURE 13. H_3O^+ rotational energy in the plane defined by the 3 hydrogen atoms of in this ion. The rotation axis is defined by the normal of this plane that passes through the oxygen atom of the hydronium ion. Energy differences are shown with respect to static equilibrium structure at zero degrees. Circles represent the calculated values. The dashed line is a guide to the eye.

FIGURE 14. Energetics of the hydronium motion. Only one hydronium was displaced. All displacements are along parallel to the normal (*N*) of the H_3 plane that passes through the oxygen atom of the H_3O^+ ion, as shown in the inset. Zero on the horizontal axis is the position of the H_3 plane for the relaxed structure. Solid squares: displacement of the H_3O^+ unit. Solid squares: displacement of the three hydrogen atoms for fixed oxygen. Dotted lines are guides to the eye. The vertical dashed line is the position when the H_3O^+ adopts a planar geometry.

Always consult and cite the final, published document. See http:/www.minsocam.org or GeoscienceWorld

This is a preprint, the final version is subject to change, of the American Mineralogist (MSA)
Cite as Authors (Year) Title. American Mineralogist, in press.
(DOI will not work until issue is live.) DOI: http://dx.doi.org/10.2138/am-2017-5909

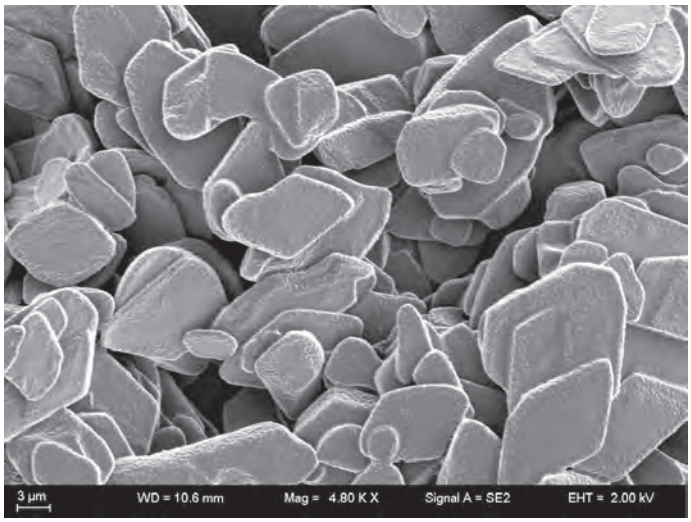

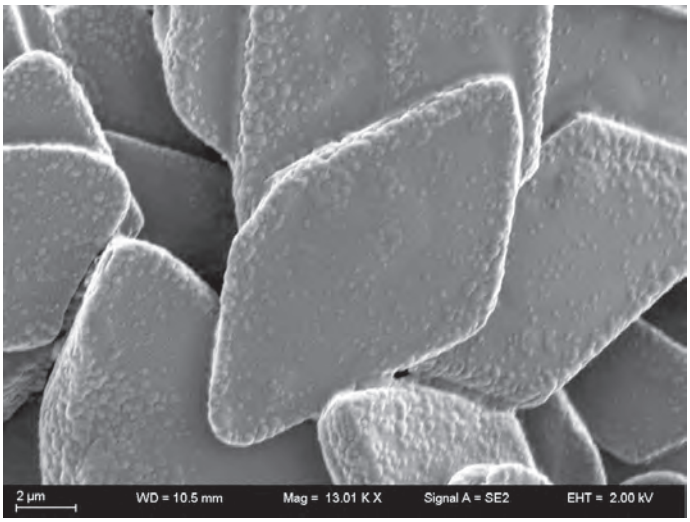

Fig. 1. Majzlan et al.: Thermodynamics of rhomboclase and ....

pp

Always consult and cite the final, published document. See http:/www.minsocam.org or GeoscienceWorld

This is a preprint, the final version is subject to change, of the American Mineralogist (MSA)
Cite as Authors (Year) Title. American Mineralogist, in press.
(DOI will not work until issue is live.) DOI: http://dx.doi.org/10.2138/am-2017-5909

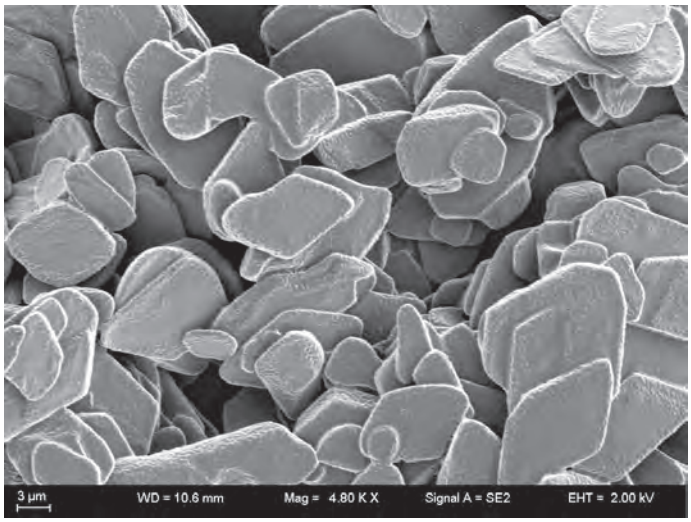

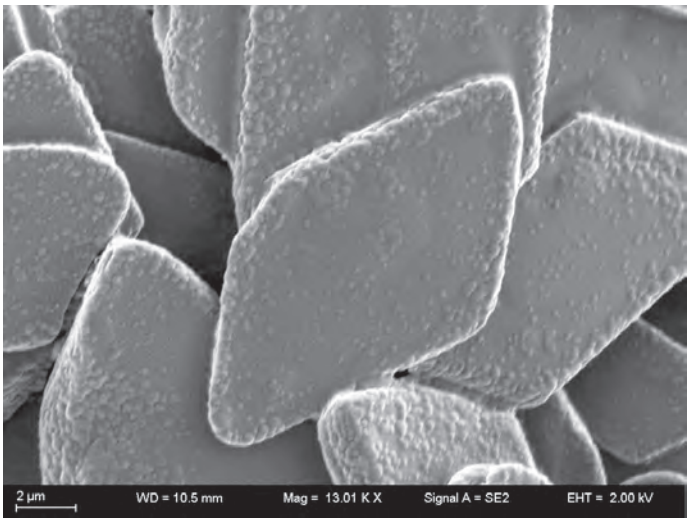

Fig. 1. Majzlan et al.: Thermodynamics of rhomboclase and ....

pp

Always consult and cite the final, published document. See http:/www.minsocam.org or GeoscienceWorld

This is a preprint, the final version is subject to change, of the American Mineralogist (MSA)
Cite as Authors (Year) Title. American Mineralogist, in press.
(DOI will not work until issue is live.) DOI: http://dx.doi.org/10.2138/am-2017-5909

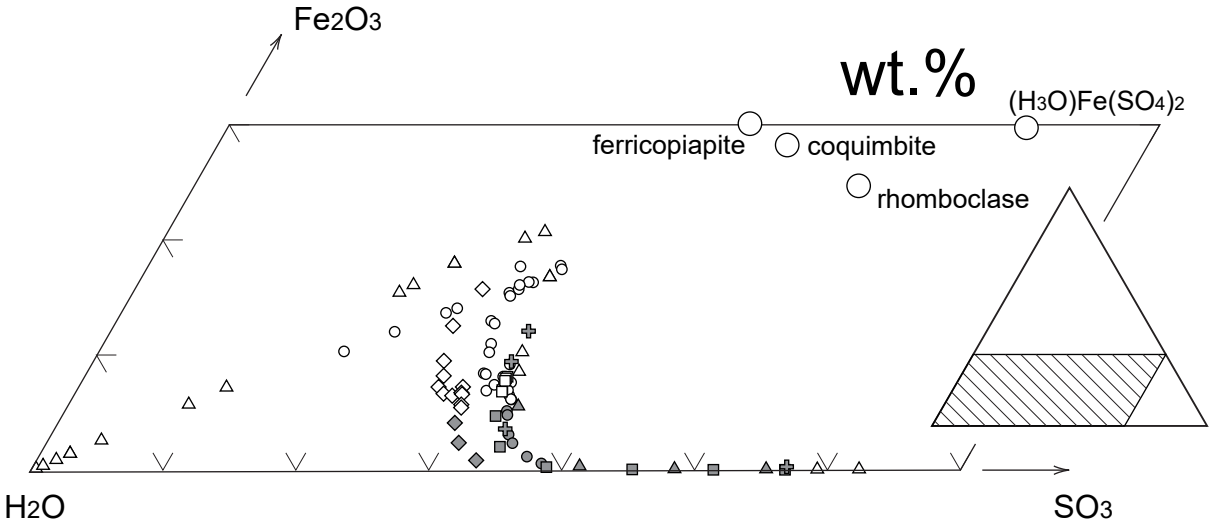

Fig. 2. Majzlan et al.: Thermodynamics of rhomboclase and ....

Always consult and cite the final, published document. See http:/www.minsocam.org or GeoscienceWorld

This is a preprint, the final version is subject to change, of the American Mineralogist (MSA)
Cite as Authors (Year) Title. American Mineralogist, in press.
(DOI will not work until issue is live.) DOI: http://dx.doi.org/10.2138/am-2017-5909

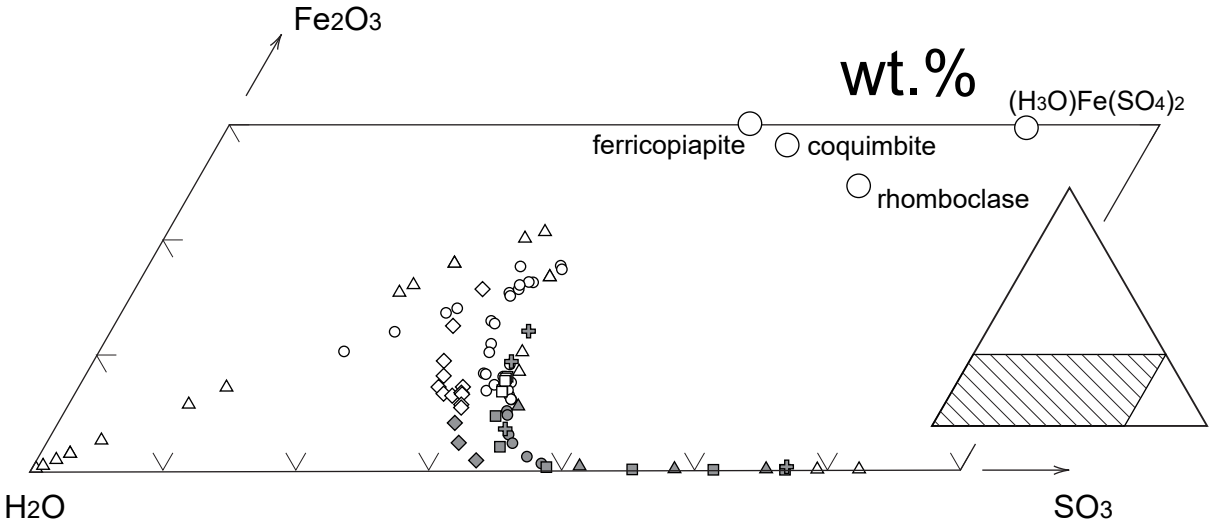

Fig. 2. Majzlan et al.: Thermodynamics of rhomboclase and ....

Always consult and cite the final, published document. See http:/www.minsocam.org or GeoscienceWorld

This is a preprint, the final version is subject to change, of the American Mineralogist (MSA)
Cite as Authors (Year) Title. American Mineralogist, in press.
(DOI will not work until issue is live.) DOI: http://dx.doi.org/10.2138/am-2017-5909

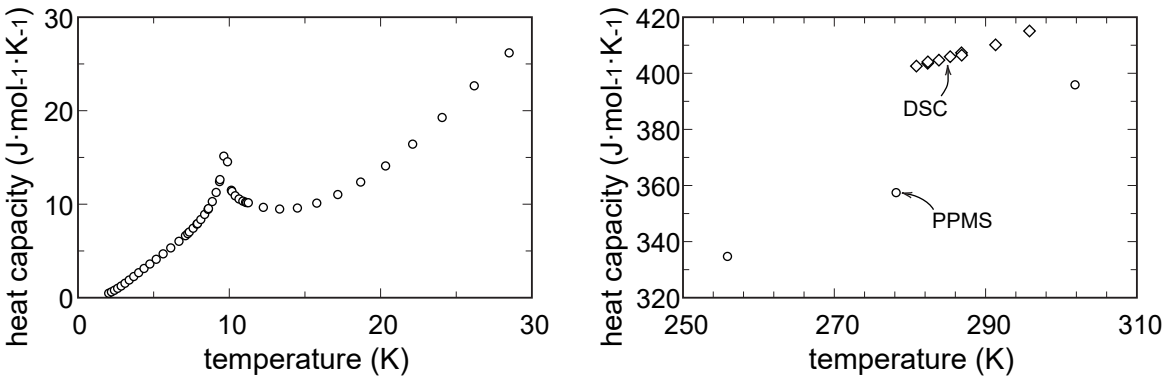

Fig. 3. Majzlan et al.: Thermodynamics of rhomboclase and ....

pp

Always consult and cite the final, published document. See http:/www.minsocam.org or GeoscienceWorld

This is a preprint, the final version is subject to change, of the American Mineralogist (MSA)
Cite as Authors (Year) Title. American Mineralogist, in press.
(DOI will not work until issue is live.) DOI: http://dx.doi.org/10.2138/am-2017-5909

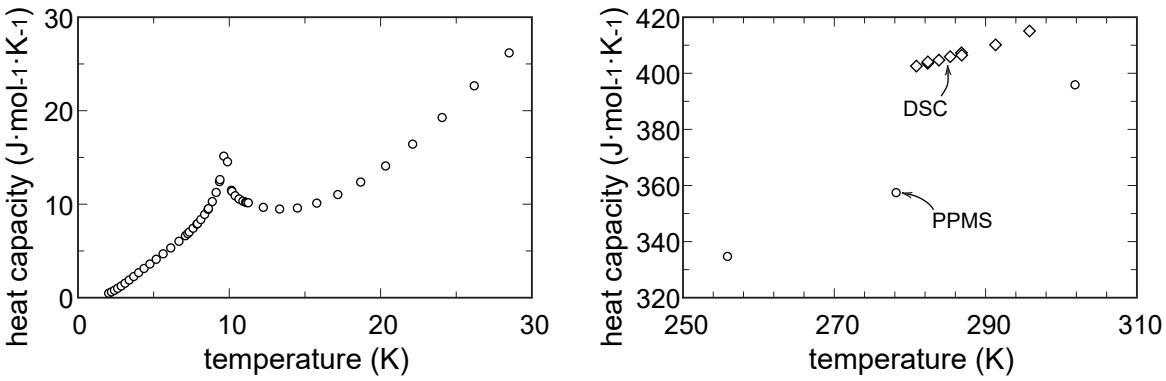

Fig. 3. Majzlan et al.: Thermodynamics of rhomboclase and ....

pp

Always consult and cite the final, published document. See http:/www.minsocam.org or GeoscienceWorld

This is a preprint, the final version is subject to change, of the American Mineralogist (MSA)
Cite as Authors (Year) Title. American Mineralogist, in press.
(DOI will not work until issue is live.) DOI: http://dx.doi.org/10.2138/am-2017-5909

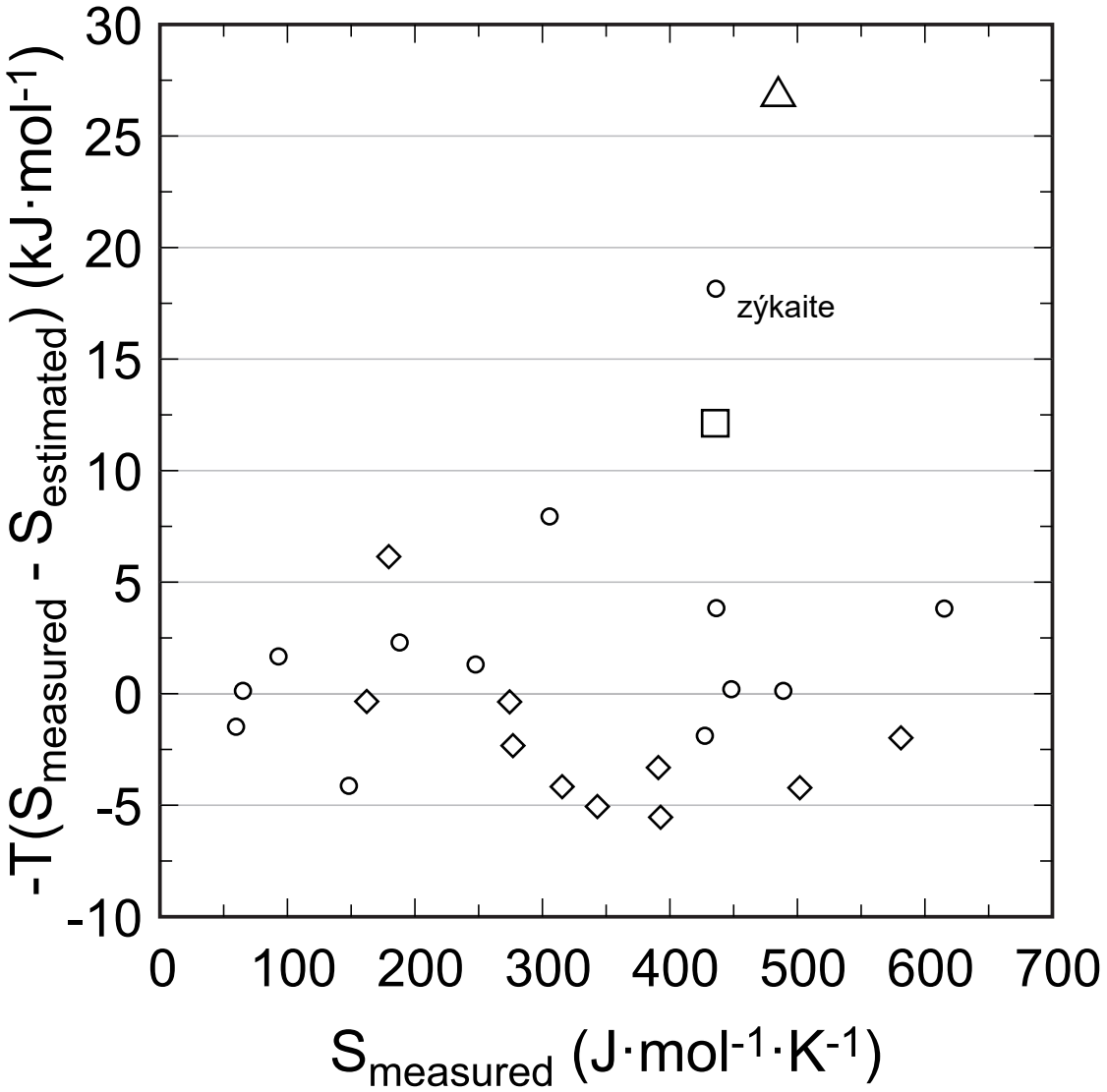

Fig. 4. Majzlan et al.: Thermodynamics of rhomboclase and ....

Always consult and cite the final, published document. See http:/www.minsocam.org or GeoscienceWorld

This is a preprint, the final version is subject to change, of the American Mineralogist (MSA)
Cite as Authors (Year) Title. American Mineralogist, in press.
(DOI will not work until issue is live.) DOI: http://dx.doi.org/10.2138/am-2017-5909

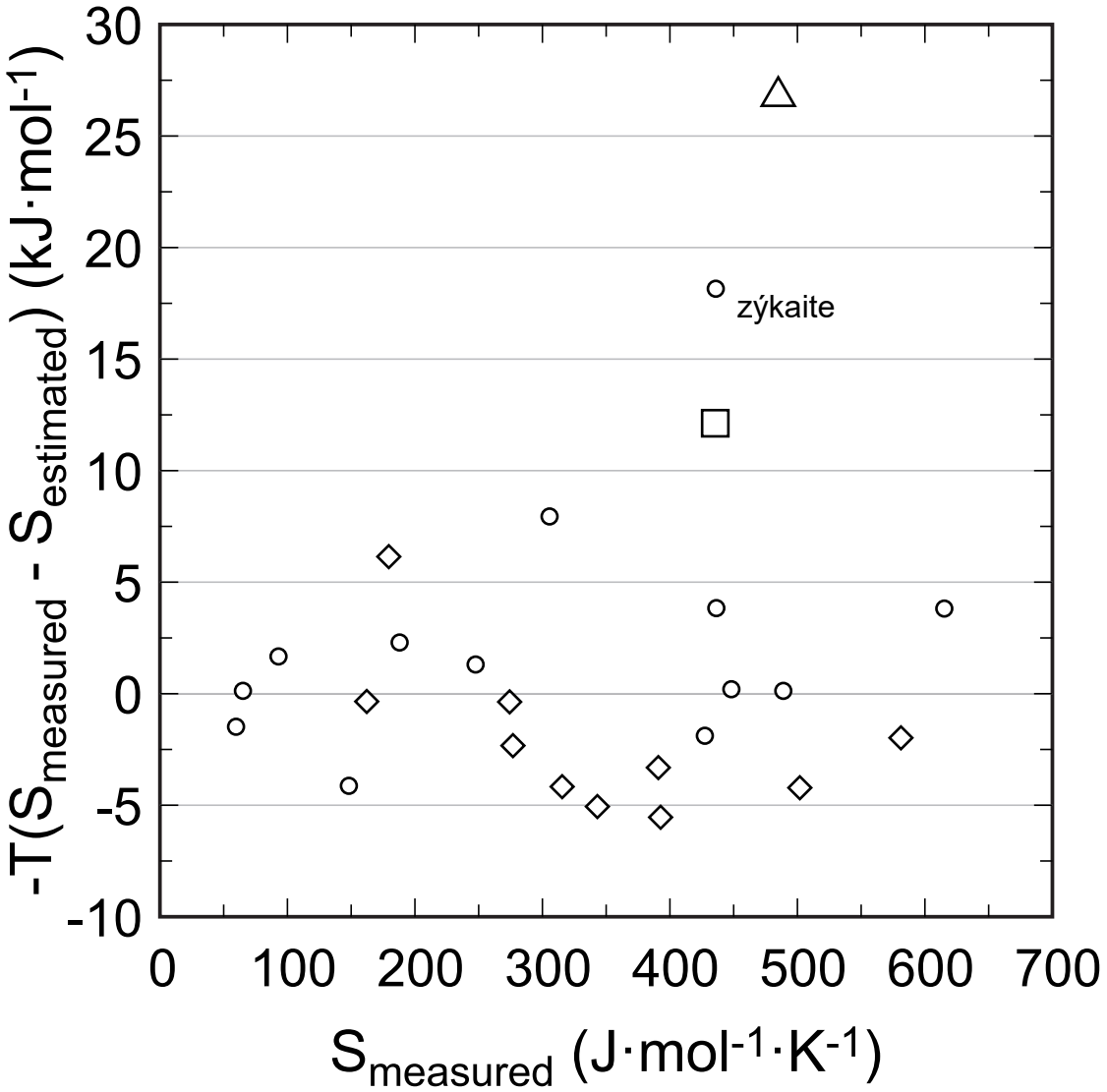

Fig. 4. Majzlan et al.: Thermodynamics of rhomboclase and ....

Always consult and cite the final, published document. See http:/www.minsocam.org or GeoscienceWorld

This is a preprint, the final version is subject to change, of the American Mineralogist (MSA)
Cite as Authors (Year) Title. American Mineralogist, in press.
(DOI will not work until issue is live.) DOI: http://dx.doi.org/10.2138/am-2017-5909

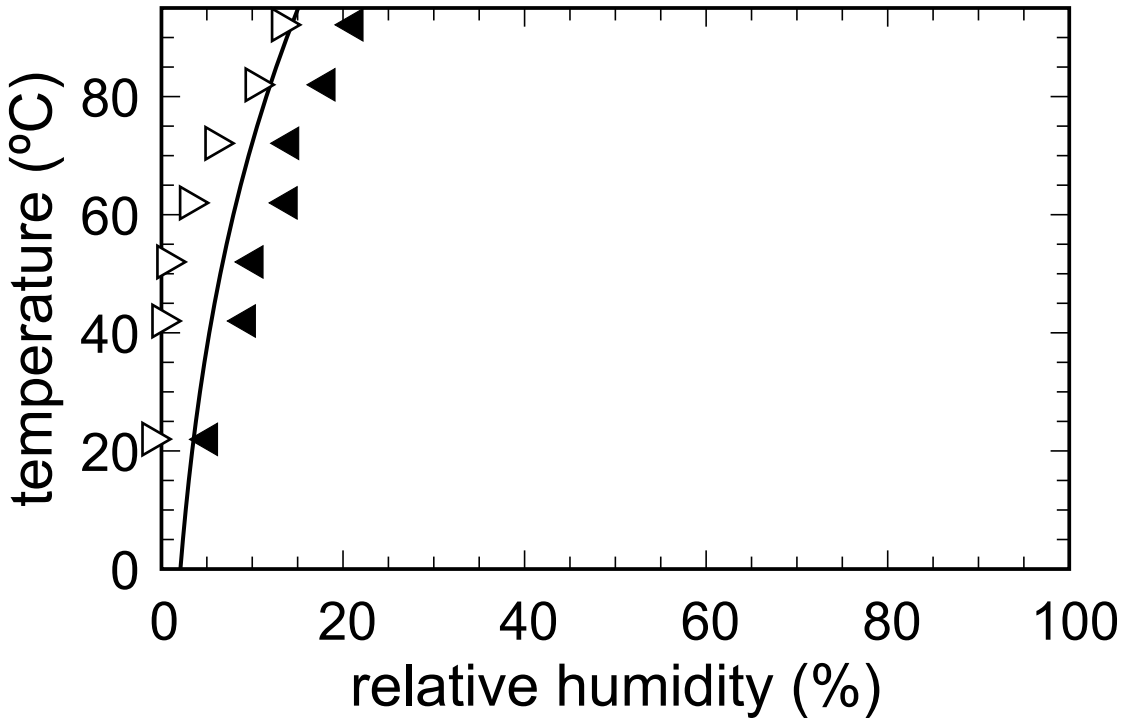

Fig. 5. Majzlan et al.: Thermodynamics of rhomboclase and ....

Always consult and cite the final, published document. See http:/www.minsocam.org or GeoscienceWorld

This is a preprint, the final version is subject to change, of the American Mineralogist (MSA)
Cite as Authors (Year) Title. American Mineralogist, in press.
(DOI will not work until issue is live.) DOI: http://dx.doi.org/10.2138/am-2017-5909

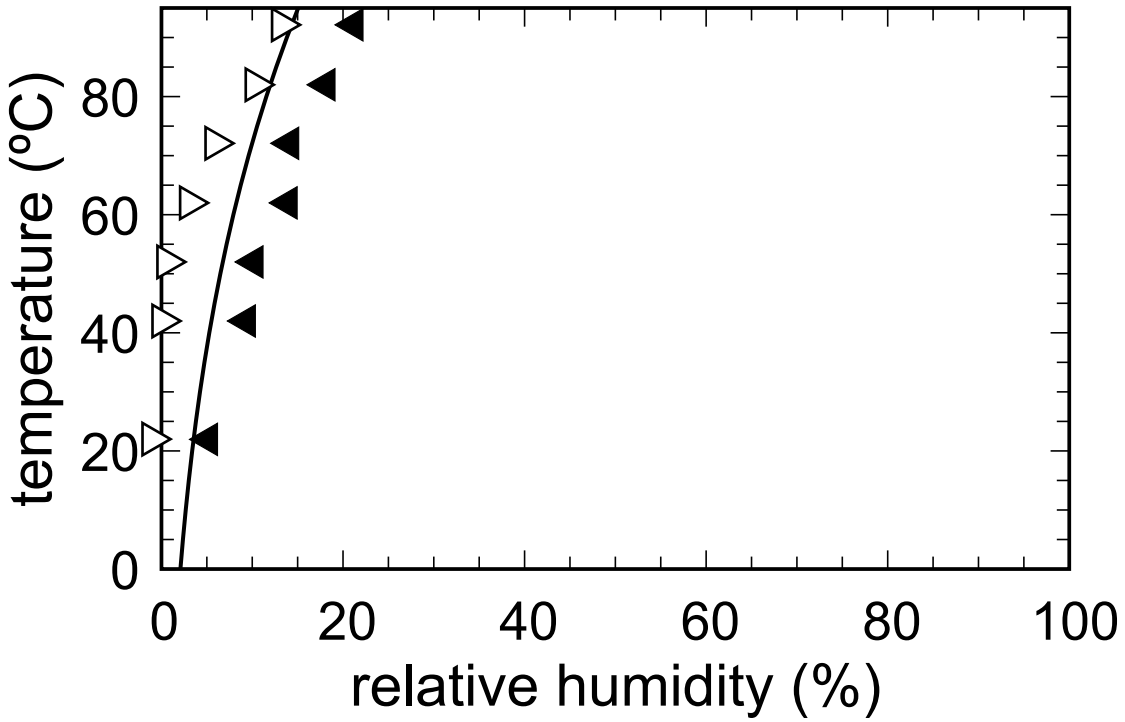

Fig. 5. Majzlan et al.: Thermodynamics of rhomboclase and ....

Always consult and cite the final, published document. See http:/www.minsocam.org or GeoscienceWorld

This is a preprint, the final version is subject to change, of the American Mineralogist (MSA)
Cite as Authors (Year) Title. American Mineralogist, in press.
(DOI will not work until issue is live.) DOI: http://dx.doi.org/10.2138/am-2017-5909

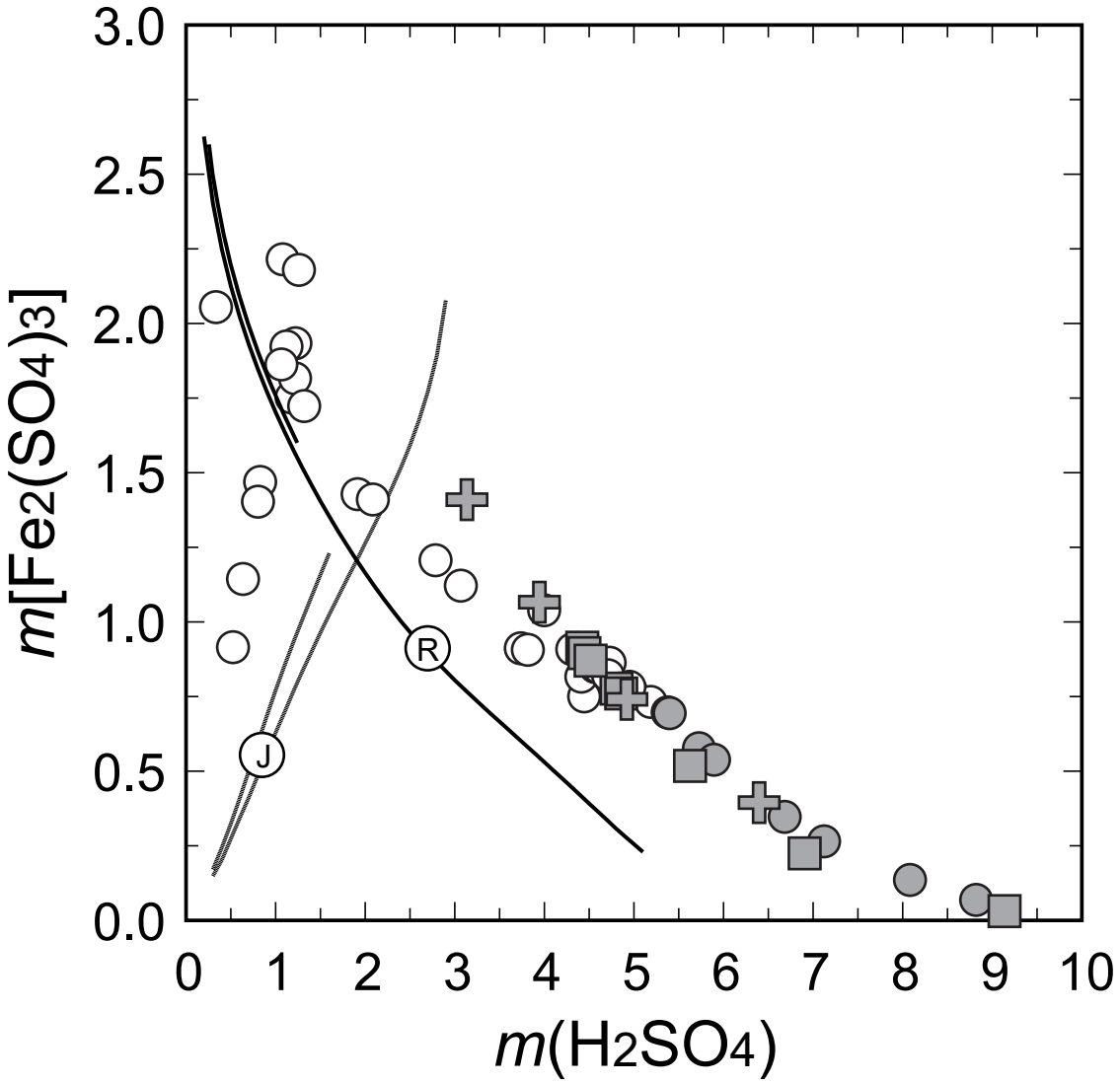

Fig. 6. Majzlan et al.: Thermodynamics of rhomboclase and ....

pp

Always consult and cite the final, published document. See http:/www.minsocam.org or GeoscienceWorld

This is a preprint, the final version is subject to change, of the American Mineralogist (MSA)
Cite as Authors (Year) Title. American Mineralogist, in press.
(DOI will not work until issue is live.) DOI: http://dx.doi.org/10.2138/am-2017-5909

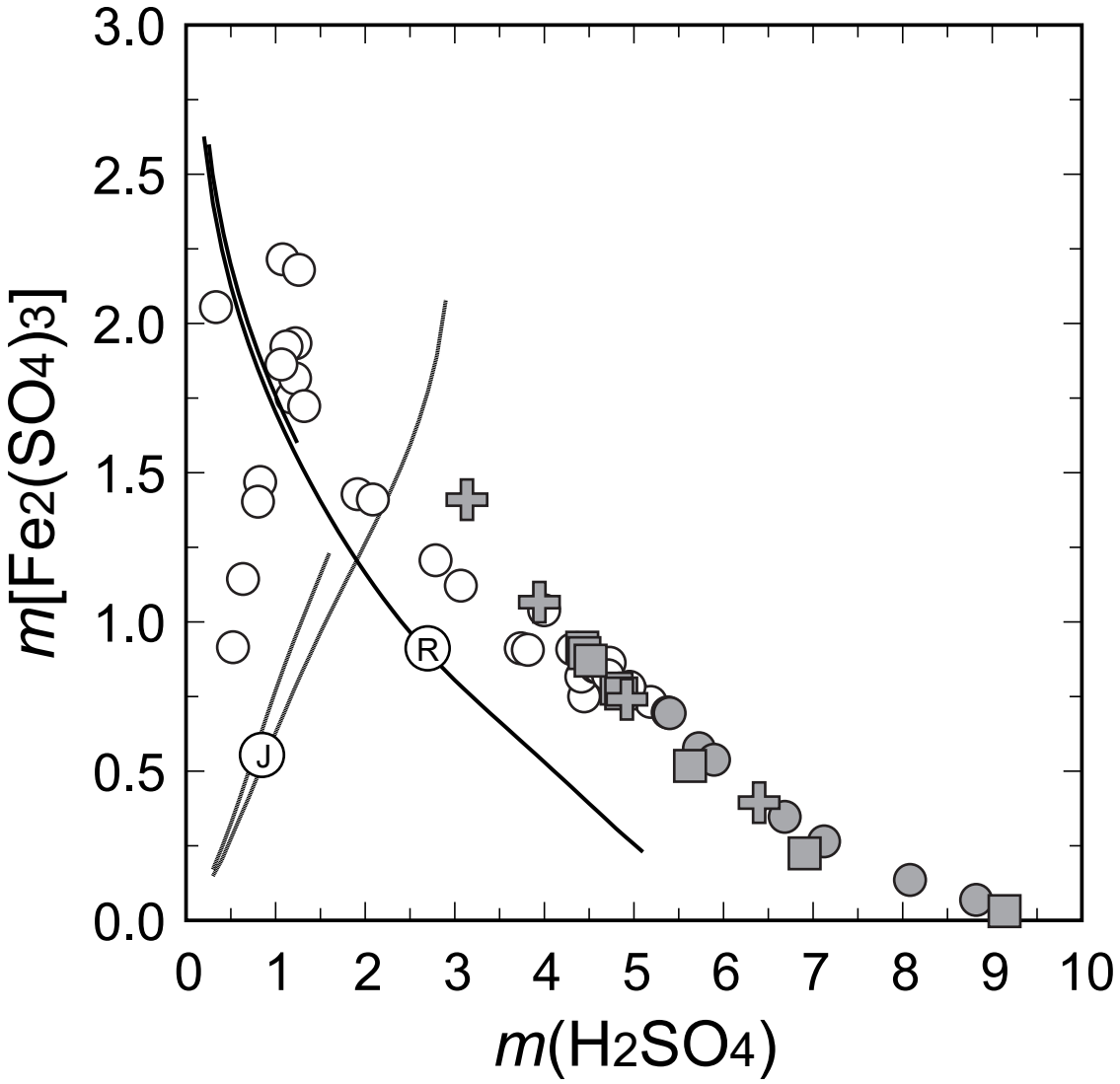

Fig. 6. Majzlan et al.: Thermodynamics of rhomboclase and ....

pp

Always consult and cite the final, published document. See http:/www.minsocam.org or GeoscienceWorld

This is a preprint, the final version is subject to change, of the American Mineralogist (MSA)
Cite as Authors (Year) Title. American Mineralogist, in press.
(DOI will not work until issue is live.) DOI: http://dx.doi.org/10.2138/am-2017-5909

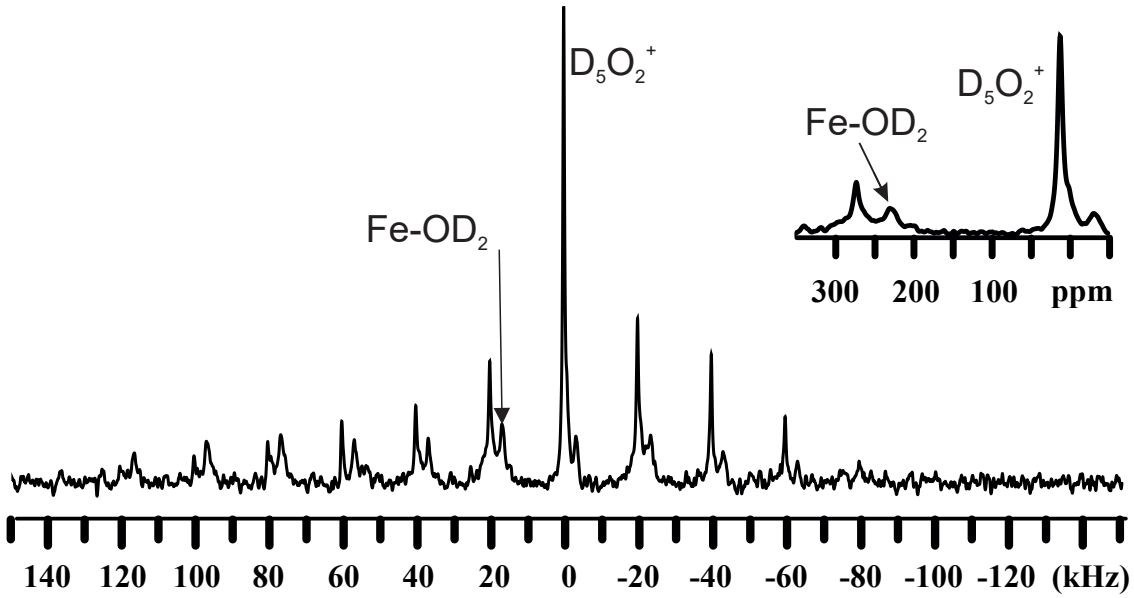

Fig. 7. Majzlan et al.: Thermodynamics of rhomboclase and ....

pp

Always consult and cite the final, published document. See http:/www.minsocam.org or GeoscienceWorld

This is a preprint, the final version is subject to change, of the American Mineralogist (MSA)
Cite as Authors (Year) Title. American Mineralogist, in press.
(DOI will not work until issue is live.) DOI: http://dx.doi.org/10.2138/am-2017-5909

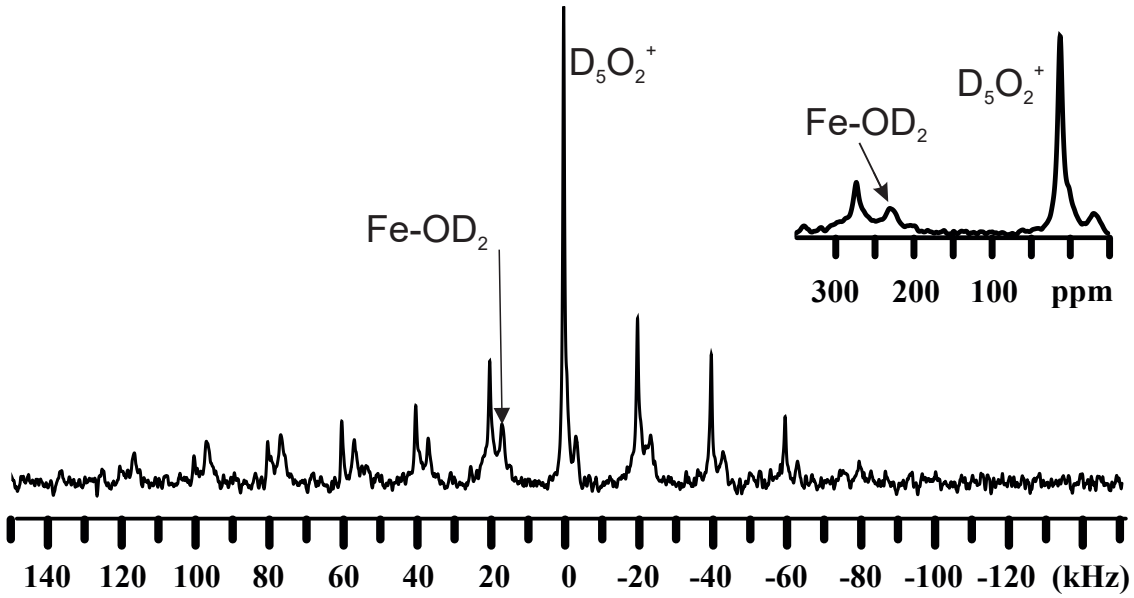

Fig. 7. Majzlan et al.: Thermodynamics of rhomboclase and ....

pp

Always consult and cite the final, published document. See http:/www.minsocam.org or GeoscienceWorld

This is a preprint, the final version is subject to change, of the American Mineralogist (MSA)
Cite as Authors (Year) Title. American Mineralogist, in press.
(DOI will not work until issue is live.) DOI: http://dx.doi.org/10.2138/am-2017-5909

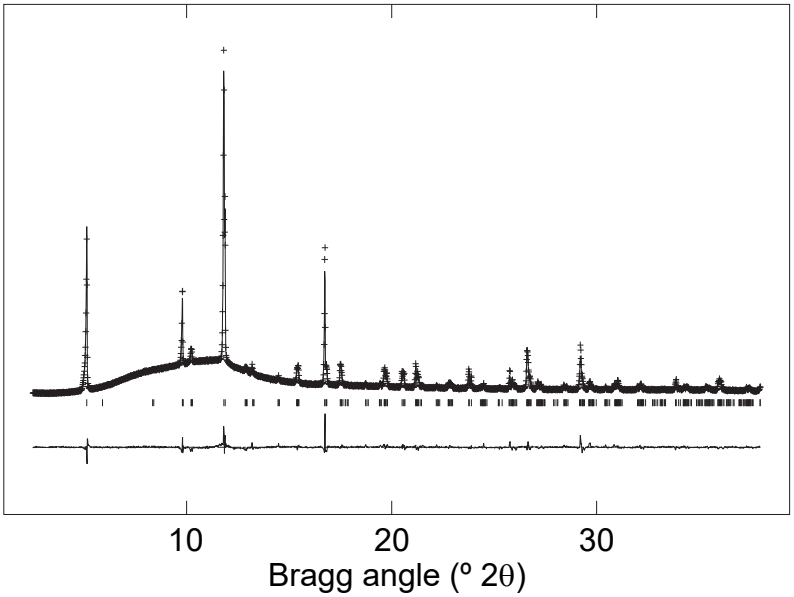

Fig. 8. Majzlan et al.: Thermodynamics of rhomboclase and ....

pp

Always consult and cite the final, published document. See http:/www.minsocam.org or GeoscienceWorld

This is a preprint, the final version is subject to change, of the American Mineralogist (MSA)
Cite as Authors (Year) Title. American Mineralogist, in press.
(DOI will not work until issue is live.) DOI: http://dx.doi.org/10.2138/am-2017-5909

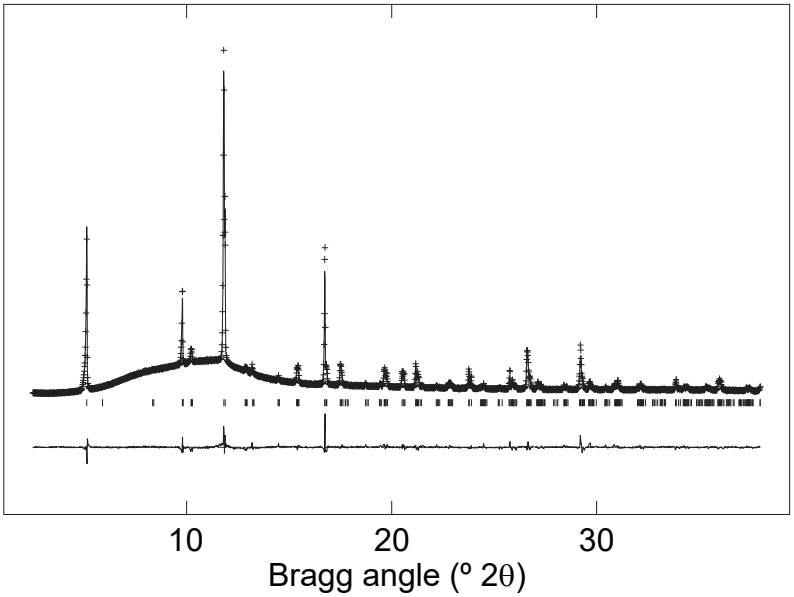

Fig. 8. Majzlan et al.: Thermodynamics of rhomboclase and ....

pp

Always consult and cite the final, published document. See http:/www.minsocam.org or GeoscienceWorld

This is a preprint, the final version is subject to change, of the American Mineralogist (MSA)
Cite as Authors (Year) Title. American Mineralogist, in press.
(DOI will not work until issue is live.) DOI: http://dx.doi.org/10.2138/am-2017-5909

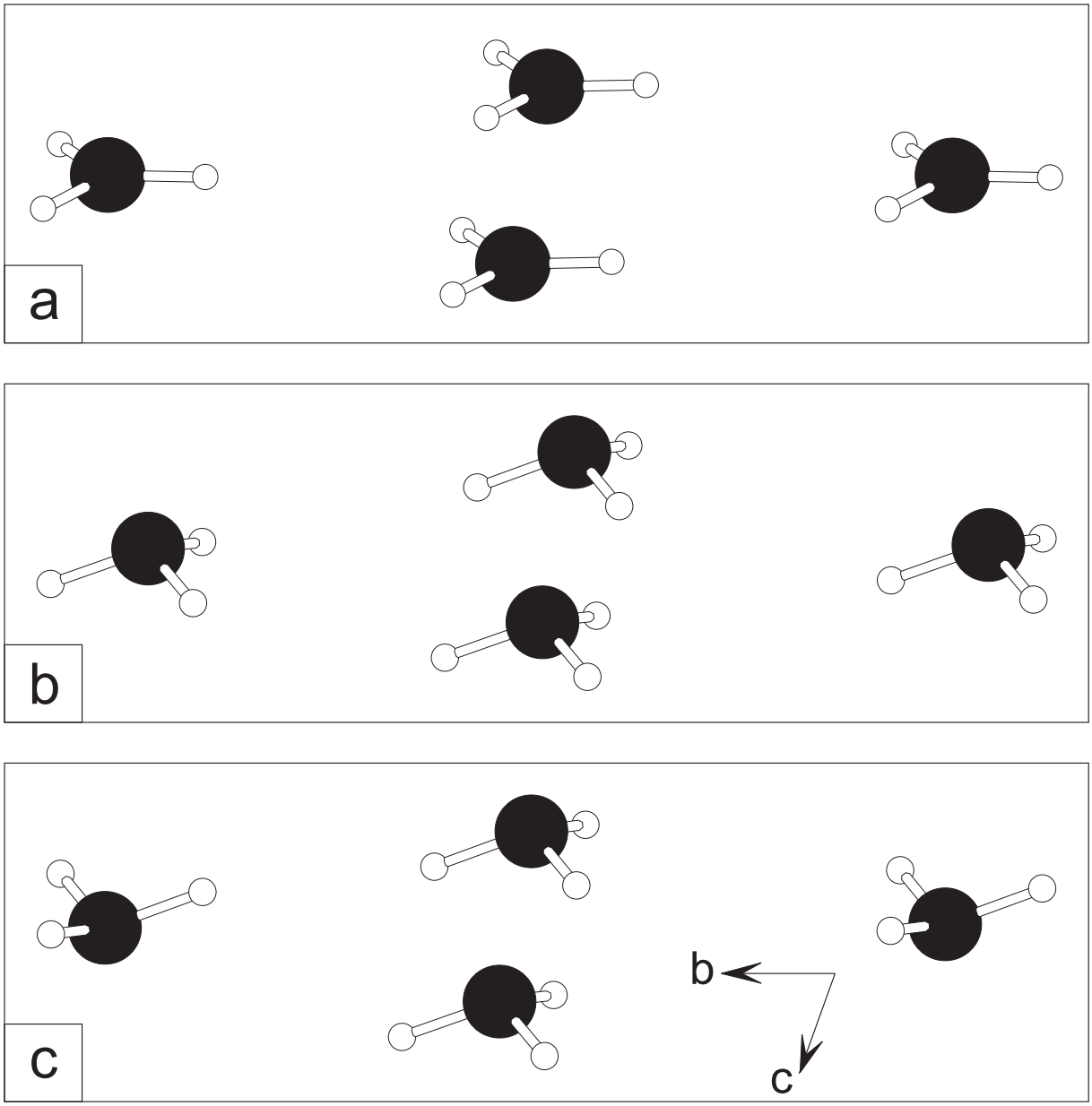

Fig. 9. Majzlan et al.: Thermodynamics of rhomboclase and ....

Always consult and cite the final, published document. See http:/www.minsocam.org or GeoscienceWorld

This is a preprint, the final version is subject to change, of the American Mineralogist (MSA)
Cite as Authors (Year) Title. American Mineralogist, in press.
(DOI will not work until issue is live.) DOI: http://dx.doi.org/10.2138/am-2017-5909

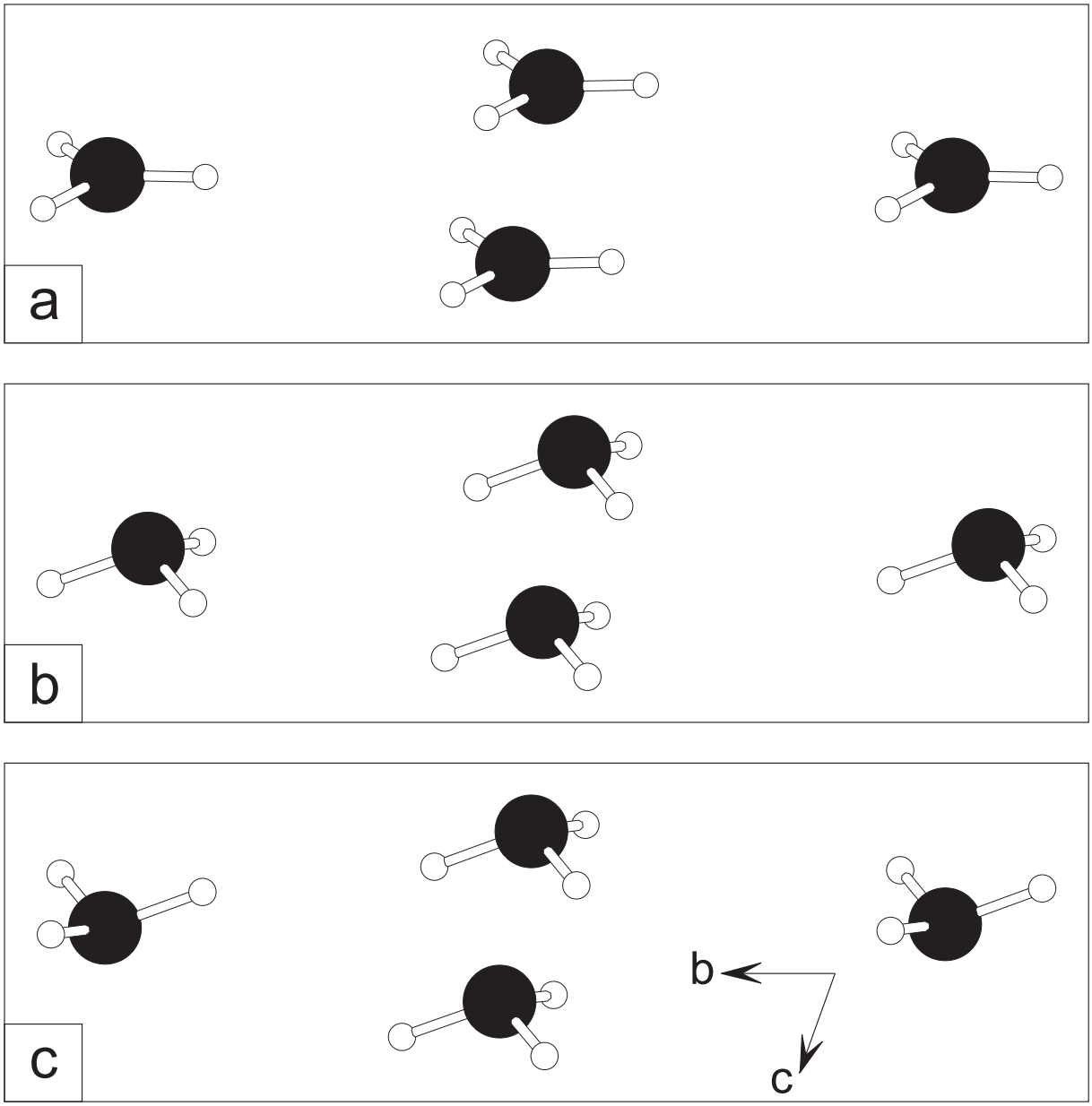

Fig. 9. Majzlan et al.: Thermodynamics of rhomboclase and ....

Always consult and cite the final, published document. See http:/www.minsocam.org or GeoscienceWorld

This is a preprint, the final version is subject to change, of the American Mineralogist (MSA)
Cite as Authors (Year) Title. American Mineralogist, in press.
(DOI will not work until issue is live.) DOI: http://dx.doi.org/10.2138/am-2017-5909

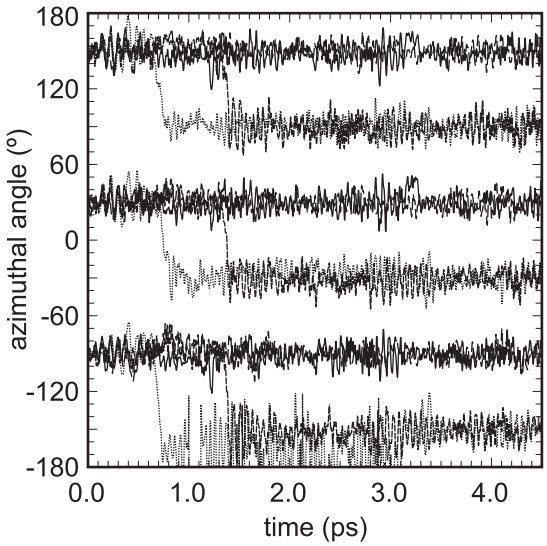

Fig. 10. Majzlan et al.: Thermodynamics of rhomboclase and ....

pp

Always consult and cite the final, published document. See http:/www.minsocam.org or GeoscienceWorld

This is a preprint, the final version is subject to change, of the American Mineralogist (MSA)
Cite as Authors (Year) Title. American Mineralogist, in press.
(DOI will not work until issue is live.) DOI: http://dx.doi.org/10.2138/am-2017-5909

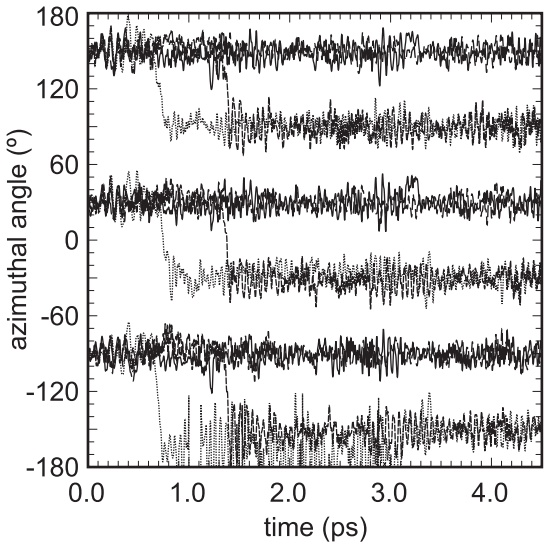

Fig. 10. Majzlan et al.: Thermodynamics of rhomboclase and ....

pp

Always consult and cite the final, published document. See http:/www.minsocam.org or GeoscienceWorld

This is a preprint, the final version is subject to change, of the American Mineralogist (MSA)
Cite as Authors (Year) Title. American Mineralogist, in press.
(DOI will not work until issue is live.) DOI: http://dx.doi.org/10.2138/am-2017-5909

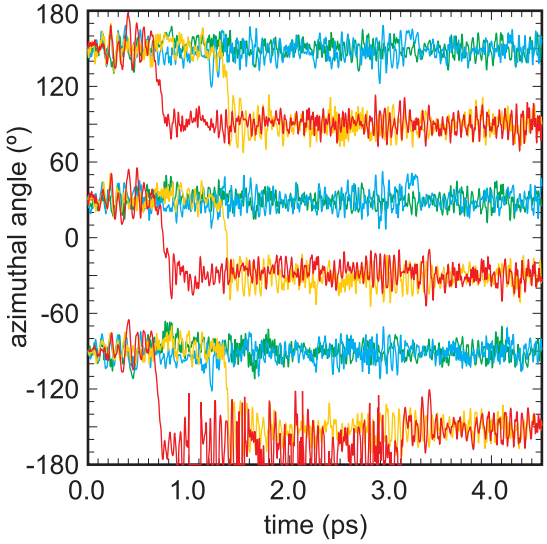

Fig. 10. Majzlan et al.: Thermodynamics of rhomboclase and ....

pp

Always consult and cite the final, published document. See http:/www.minsocam.org or GeoscienceWorld

This is a preprint, the final version is subject to change, of the American Mineralogist (MSA)
Cite as Authors (Year) Title. American Mineralogist, in press.
(DOI will not work until issue is live.) DOI: http://dx.doi.org/10.2138/am-2017-5909

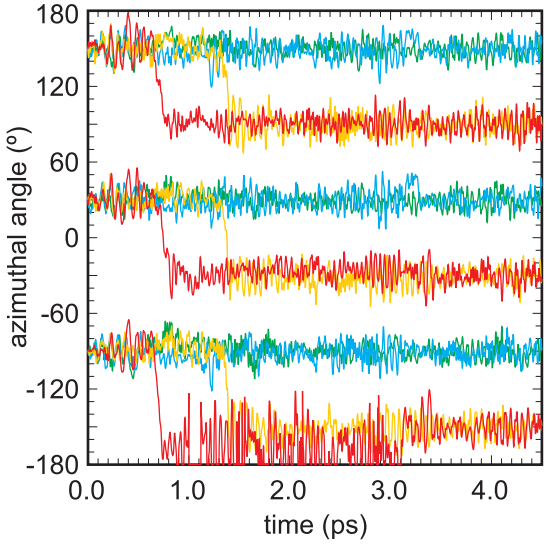

Fig. 10. Majzlan et al.: Thermodynamics of rhomboclase and ....

pp

Always consult and cite the final, published document. See http:/www.minsocam.org or GeoscienceWorld

This is a preprint, the final version is subject to change, of the American Mineralogist (MSA)
Cite as Authors (Year) Title. American Mineralogist, in press.
(DOI will not work until issue is live.) DOI: http://dx.doi.org/10.2138/am-2017-5909

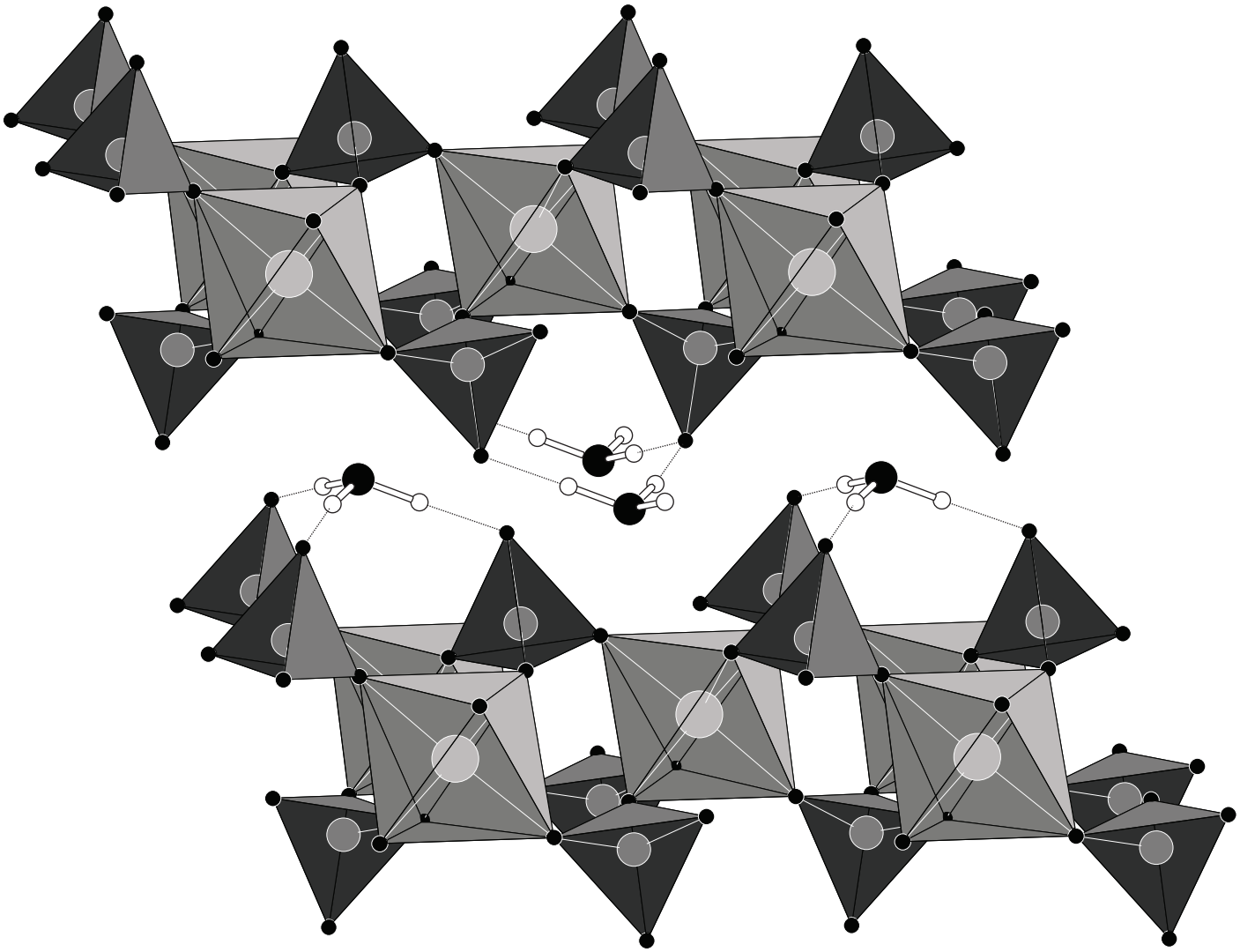

Fig. 11. Majzlan et al.: Thermodynamics of rhomboclase and ....

pp

Always consult and cite the final, published document. See http:/www.minsocam.org or GeoscienceWorld

This is a preprint, the final version is subject to change, of the American Mineralogist (MSA)
Cite as Authors (Year) Title. American Mineralogist, in press.
(DOI will not work until issue is live.) DOI: http://dx.doi.org/10.2138/am-2017-5909

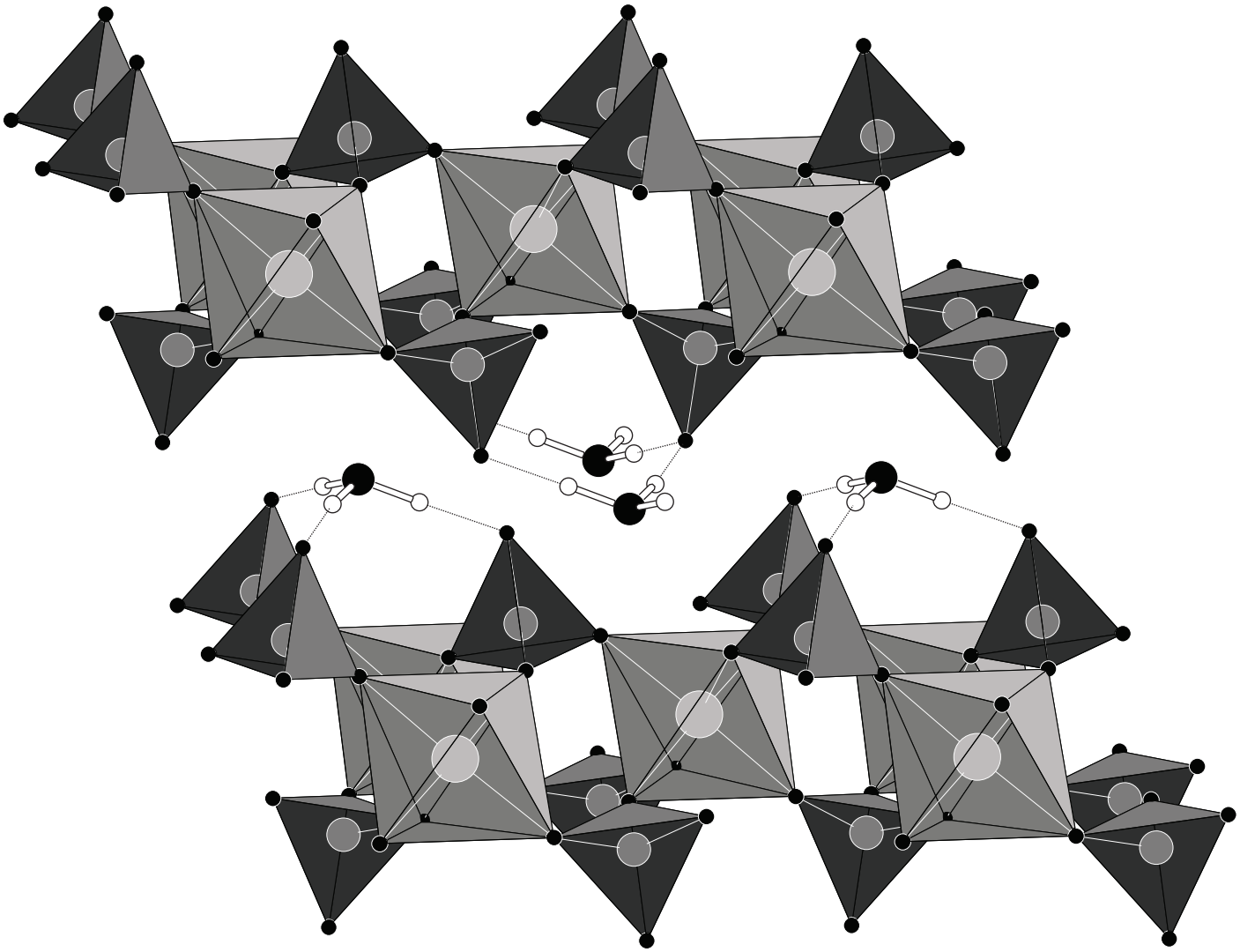

Fig. 11. Majzlan et al.: Thermodynamics of rhomboclase and ....

pp

Always consult and cite the final, published document. See http:/www.minsocam.org or GeoscienceWorld

This is a preprint, the final version is subject to change, of the American Mineralogist (MSA)
Cite as Authors (Year) Title. American Mineralogist, in press.
(DOI will not work until issue is live.) DOI: http://dx.doi.org/10.2138/am-2017-5909

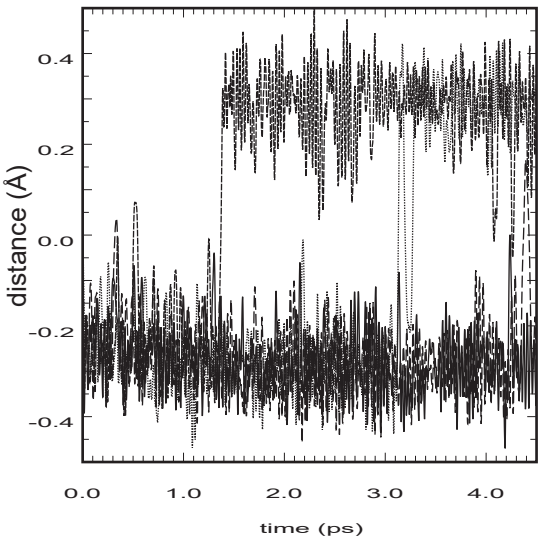

Fig. 12. Majzlan et al.: Thermodynamics of rhomboclase and ....

pp

Always consult and cite the final, published document. See http:/www.minsocam.org or GeoscienceWorld

This is a preprint, the final version is subject to change, of the American Mineralogist (MSA)
Cite as Authors (Year) Title. American Mineralogist, in press.
(DOI will not work until issue is live.) DOI: http://dx.doi.org/10.2138/am-2017-5909

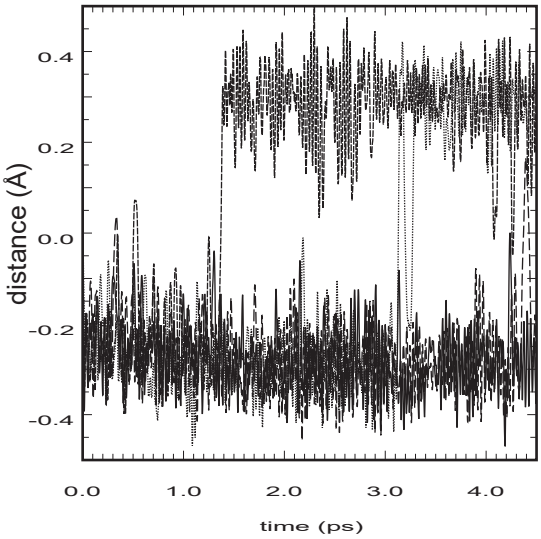

Fig. 12. Majzlan et al.: Thermodynamics of rhomboclase and ....

pp

Always consult and cite the final, published document. See http:/www.minsocam.org or GeoscienceWorld

This is a preprint, the final version is subject to change, of the American Mineralogist (MSA)
Cite as Authors (Year) Title. American Mineralogist, in press.
(DOI will not work until issue is live.) DOI: http://dx.doi.org/10.2138/am-2017-5909

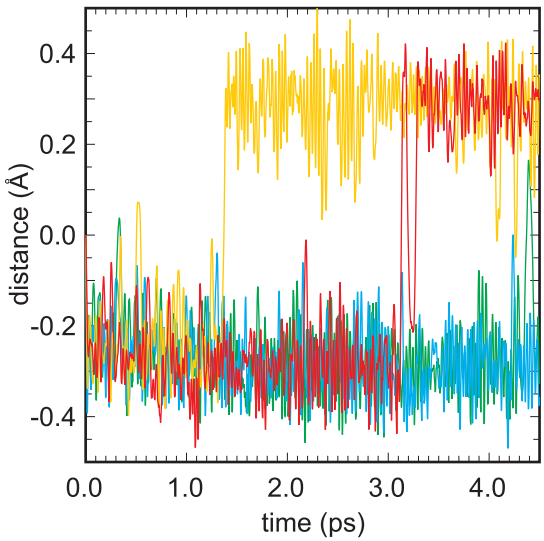

Fig. 12. Majzlan et al.: Thermodynamics of rhomboclase and ....

Always consult and cite the final, published document. See http:/www.minsocam.org or GeoscienceWorld

This is a preprint, the final version is subject to change, of the American Mineralogist (MSA)
Cite as Authors (Year) Title. American Mineralogist, in press.
(DOI will not work until issue is live.) DOI: http://dx.doi.org/10.2138/am-2017-5909

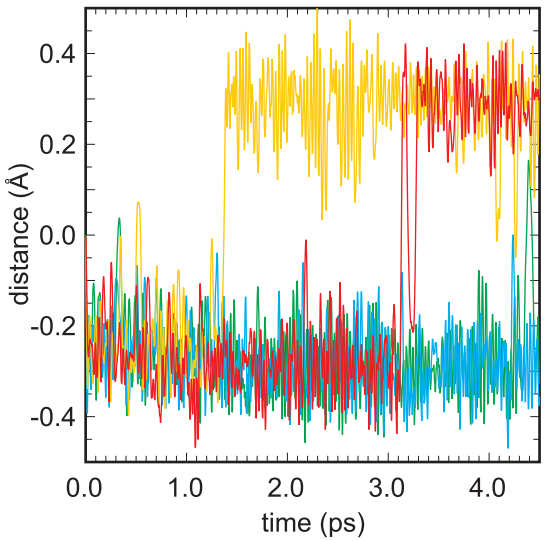

Fig. 12. Majzlan et al.: Thermodynamics of rhomboclase and ....

Always consult and cite the final, published document. See http:/www.minsocam.org or GeoscienceWorld

This is a preprint, the final version is subject to change, of the American Mineralogist (MSA)
Cite as Authors (Year) Title. American Mineralogist, in press.
(DOI will not work until issue is live.) DOI: http://dx.doi.org/10.2138/am-2017-5909

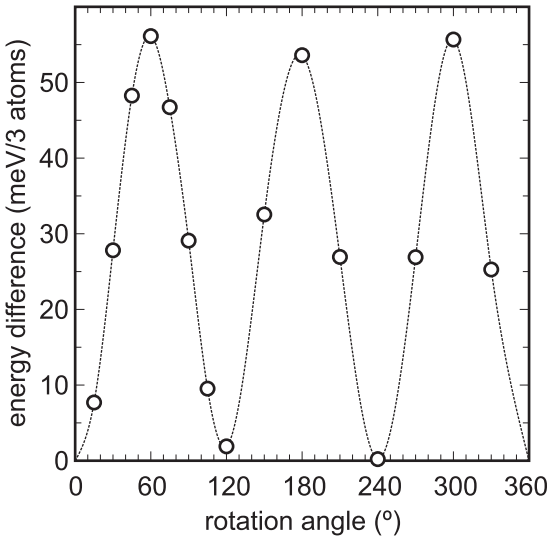

Fig. 13. Majzlan et al.: Thermodynamics of rhomboclase and ....

pp

Always consult and cite the final, published document. See http:/www.minsocam.org or GeoscienceWorld

This is a preprint, the final version is subject to change, of the American Mineralogist (MSA)
Cite as Authors (Year) Title. American Mineralogist, in press.
(DOI will not work until issue is live.) DOI: http://dx.doi.org/10.2138/am-2017-5909

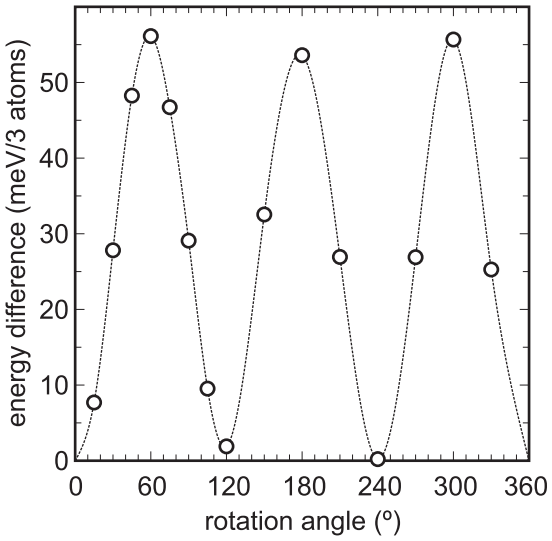

Fig. 13. Majzlan et al.: Thermodynamics of rhomboclase and ....

pp

Always consult and cite the final, published document. See http:/www.minsocam.org or GeoscienceWorld

This is a preprint, the final version is subject to change, of the American Mineralogist (MSA)
Cite as Authors (Year) Title. American Mineralogist, in press.
(DOI will not work until issue is live.) DOI: http://dx.doi.org/10.2138/am-2017-5909

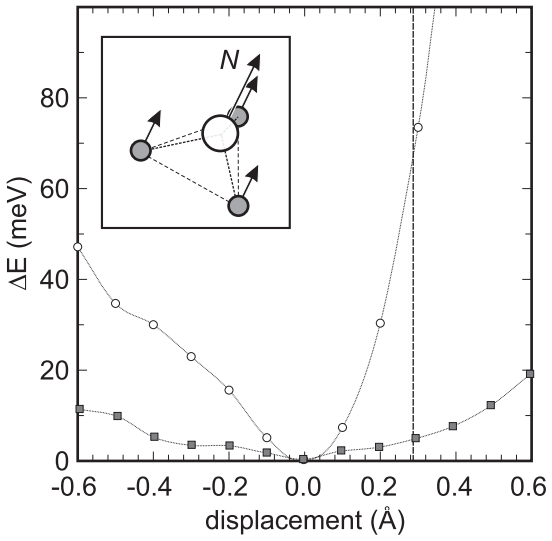

Fig. 14. Majzlan et al.: Thermodynamics of rhomboclase and ....

pp

Always consult and cite the final, published document. See http:/www.minsocam.org or GeoscienceWorld

This is a preprint, the final version is subject to change, of the American Mineralogist (MSA)
Cite as Authors (Year) Title. American Mineralogist, in press.
(DOI will not work until issue is live.) DOI: http://dx.doi.org/10.2138/am-2017-5909

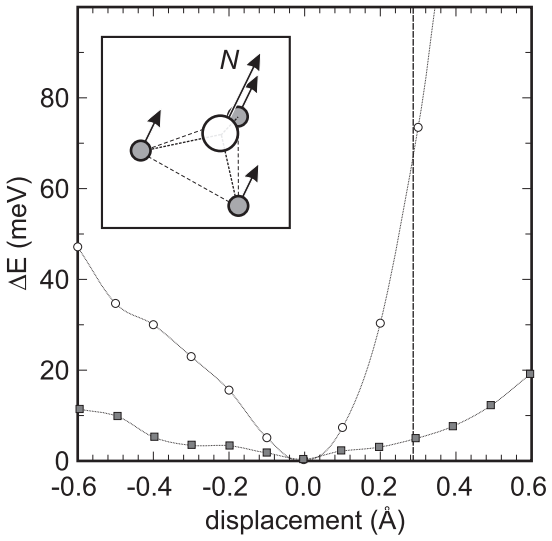

Fig. 14. Majzlan et al.: Thermodynamics of rhomboclase and ....

pp

Always consult and cite the final, published document. See http:/www.minsocam.org or GeoscienceWorld